Melting phase relations of model carbonated peridotite from 2 to 3 GPa in the system CaO-MgO-Al2O3-SiO2-CO2 and further indication of possible unmixing between carbonatite and silicate liquids

Davide Novella, Shantanu Keshav, Gudmundur H. Gudfinnsson, Shaunak Ghosh

AGU PUBLICATIONS

JGR

Journal of Geophysical Research: Solid Earth

RESEARCH ARTICLE
10.1002/2013JB010913

Key Points:
- Phase equilibria of carbonated peridotite solidus ledge
- Carbonatites along the solidus ledge
- Possible liquid immiscibility between carbonatite and silicate liquids

Correspondence to:
S. Keshav,
keshav@gm.univ-montp2.fr

Citation:
Novella, D., S. Keshav, G. H. Gudfinnsson, and S. Ghosh (2014), Melting phase relations of model carbonated peridotite from 2 to 3 GPa in the system CaO-MgO-Al_2O_3-SiO_2-CO_2 and further indication of possible unmixing between carbonatite and silicate liquids, *J. Geophys. Res. Solid Earth*, *119*, 2780–2800, doi:10.1002/2013JB010913.

Received 11 DEC 2013
Accepted 30 JAN 2014
Accepted article online 4 FEB 2014
Published online 11 APR 11
Corrected 18 JUN 2014

This article was corrected on 18 JUN 2014. See the end of the full text for details.

Melting phase relations of model carbonated peridotite from 2 to 3 GPa in the system CaO-MgO-Al_2O_3-SiO_2-CO_2 and further indication of possible unmixing between carbonatite and silicate liquids

Davide Novella[1], Shantanu Keshav[1,2], Gudmundur H. Gudfinnsson[3,4], and Shaunak Ghosh[5,6]

[1]Bayerisches Geoinstitut, Universität Bayreuth, Bayreuth, Germany, [2]Now at Geosciences Montpellier, University of Montpellier 2, CNRS & UMR 5243, Montpellier, France, [3]Iceland GeoSurvey, Reykjavik, Iceland, [4]Now at Institute of Earth Sciences, University of Iceland, Reykjavik, Iceland, [5]Department of Geology and Geophysics, Indian Institute of Technology, Kharagpur, West Bengal, India, [6]Now at Jackson School of Geosciences, University of Texas at Austin, Austin, Texas, USA

Abstract Melting phase relations of model carbonated peridotite in the system CaO-MgO-Al_2O_3-SiO_2-CO_2 from 2 to 3 GPa are reported. Experimentally produced melts, which are model carbonatites, with approximately 36–40 wt % CaO, 12–17 wt % MgO, 0.2–1.5 wt % Al_2O_3, 1–4 wt % SiO_2, and 40–42 wt % CO_2 (carbon dioxide) are present at all pressures investigated. At 2.8 and 3 GPa, carbonatitic melts are seen experimentally at temperatures that are very close to the vapor-free (CO_2) peridotite solidus and are found in equilibrium with forsterite, orthopyroxene, clinopyroxene, and garnet. Solidus phase relations with isobaric and pressure-temperature invariant points, defining the so-called carbonated peridotite solidus ledge, are also reported from 2.1 to 3 GPa. A divariant region exists from 2 to 2.6 GPa wherein two, compositionally different melts are present. In this region, these two melts, carbonatitic and silicate in composition, coexist with crystalline phase assemblage and free vapor. The silicate liquid has approximately 30–48 wt % SiO_2 and approximately 6 to 20 wt % of dissolved CO_2. The presence of carbonatitic and silicate liquids is interpreted to be due to liquid immiscibility. On the basis of melting phase relations reported here, we conclude that (a) the ledge is a feature along which model carbonatitic liquids are produced by reaction of silicates and CO_2 vapor and (b) alkali-free carbonatites and silicate melts can form through melt unmixing at depths of ~60–80 km in the Earth's mantle.

1. Introduction

In a recent study, *Keshav and Gudfinnsson* [2013] investigated experimentally the solidus phase relations of model, carbon dioxide (CO_2) vapor-bearing peridotite from 1.1 to 2.1 GPa in the system CaO-MgO-Al_2O_3-SiO_2-CO_2 (CMAS-CO_2). The purpose of their work was to clarify melting phase relations along the so-called carbonated peridotite solidus ledge (simply ledge or solidus ledge from now on) in CMAS-CO_2 by approaching it from the low pressure side and perhaps understand experimentally the genesis of carbonatites and the transition between silicate and carbonatitic liquids. The ledge is the most prominent feature along the solidus of carbonated peridotite (Figure 1), with fusion temperatures of carbonated peridotite in the system CaO-MgO-SiO_2-CO_2 (CMS-CO_2) decreasing, relative to the solidus of dry peridotite, by about 200–250 °C [*Eggler*, 1974, 1976; *Wyllie and Huang*, 1976a, 1976b; reviewed in *Dalton and Presnall*, 1998; *Luth*, 1999, 2006].

In the study of *Keshav and Gudfinnsson* [2013], from 1.1 to 1.9 GPa, liquid in equilibrium with forsterite, orthopyroxene (opx), clinopyroxene (cpx), spinel, and vapor is silicate in composition. This assemblage defines the pressure (P) and temperature (T) univariant solidus of model peridotite in the system CMAS-CO_2, and from 1.1 to 2 GPa, the univariant fusion curve has a positive slope in P-T space. These authors also mention that texturally, from 1.1 to 1.9 GPa, experimental charges are relatively simple to interpret. At 2 GPa, however, the quenched experimental charges seem to have two compositionally different liquids, either at or just slightly above the solidus of vapor-bearing model peridotite in the system CMAS-CO_2. These liquids are carbonatitic and silicate in compositions. The appearance of two liquids in equilibrium with forsterite, opx, cpx, spinel, and vapor causes the solidus at 2 GPa to be P-T invariant. According to *Keshav and Gudfinnsson* [2013], this P-T invariance at the solidus topology arises incidentally just when the ledge in CMAS-CO_2 is beginning to appear (see the constructs in *Dalton and Presnall* [1998] and *Gudfinnsson and Presnall* [2005])

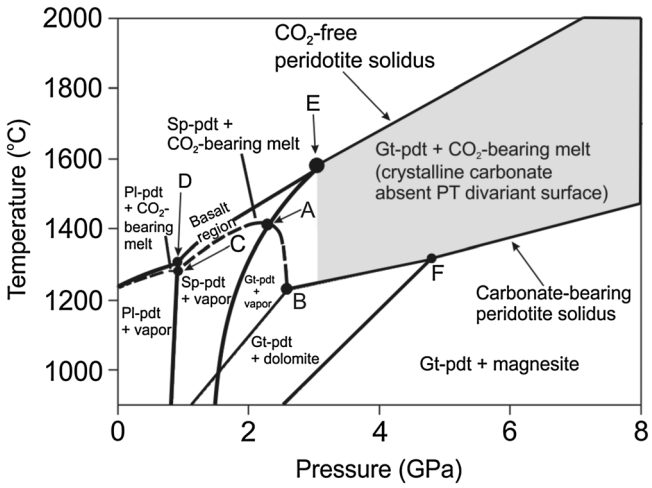

Figure 1. Solidus curves for volatile-free (CaO-MgO-Al_2O_3-SiO_2; CMAS) and carbonated (CMAS-CO_2) peridotite. The dashed curve shows the approximate location of carbonated peridotite solidus, along which CO_2 vapor (vapor) coexists with liquid and crystalline phase assemblage. A part of this dashed curve from 1.1 to 2 GPa has now been experimentally determined in the companion study [*Keshav and Gudfinnsson*, 2013] (also see the companion study for other details on this diagram). The carbonate ledge between points A and B, as drawn in *Dalton and Presnall* [1998] is a part of this dashed curve. The grey surface is from *Gudfinnsson and Presnall* [2005]. The "CO_2-free peridotite solidus" and the two P-T invariant points "D" and "E" are from *Presnall et al.* [1979], *Gudfinnsson and Presnall* [1996], *Milholland and Presnall* [1998], and *Liu and Presnall* [2000] in the system CMAS. The dashed curve between points labeled A and B and part of the P-T divariant surface approximately bounded between the P-T invariant points, "D-C-B-A-E" from 2 to 3 GPa is not known and is the focus of the present study.

and actually might be causing the ledge to appear in the first place. At 2.1 GPa, however, there is only one liquid which is in equilibrium with forsterite, opx, cpx, spinel, and vapor and is carbonatitic in composition, and the solidus between 2 and 2.1 GPa has a negative slope in P-T space [*Keshav and Gudfinnsson*, 2013]. Thus, somewhere between 2 and 2.1 GPa phase relations change so that the solidus curve along the ledge again becomes univariant in P-T space. The observation that the liquid is carbonatitic in composition at pressure as low as 2.1 GPa along the ledge in CMAS-CO_2 is contrary to previous studies in the system CMS-CO_2 [*Eggler*, 1976; *Eggler et al*., 1976; *Eggler*, 1978, 1987a, 1987b; *Wyllie and Huang*, 1976a, 1976b; *Wyllie*, 1987a, 1987b; *White and Wyllie*, 1992]. It may be that addition of alumina (Al_2O_3) to CMS-CO_2 (previous studies) causes carbonatites to appear at 2.1 GPa along the ledge.

Here we explore further the melting phase relations of model carbonated peridotite from 2 to 3 GPa in the system CMAS-CO_2. The primary considerations that precipitated the present study are as follows: (1) the solidus ledge in the system CMAS-CO_2 has never been mapped in its entirety; (2) liquid compositions in equilibrium with the relevant phase assemblage along and in the vicinity of the ledge have not been determined. When the ledge develops in the system CMS-CO_2, liquid compositions and CO_2 concentrations in the liquids have been inferred or derived through geometrical means (20–25 wt % CO_2 - Eggler and coworkers versus ~40 wt % CO_2 - Wyllie and coworkers [*Woermann and Rosenhauer*, 1985]; reviewed in *Luth* [1999, 2006]); (3) the lowest pressure at which carbonatites are experimentally produced in equilibrium with mantle peridotite is not known; and (4) does the occurrence of two liquids in the companion study [*Keshav and Gudfinnsson*, 2013] happen only at 2 GPa?

2. Methods

The experiments were conducted using several different starting mixtures (Table 1). Compositions labeled JADSCM-3, JADSCM-7, JADSCM-8, and CMAS-CO_2-1 were reproduced on the basis of compositions used in *Dalton and Presnall* [1998] and *Gudfinnsson and Presnall* [2005]. These many starting mixtures (Table 1) had to be prepared because the idea was to hold the liquid in equilibrium with a model carbonated mantle peridotite assemblage at all P-T conditions. The starting mixtures were prepared using the following ingredients: $CaCO_3$ (Alfa Aesar®, 99.998%), MgO (Alfa Aesar®, 99.998%), Al_2O_3 (Alfa Aesar®, 99.998%), SiO_2 (Aldrich®, 99.995%), and crystalline magnesite, $MgCO_3$ (Krantz®, Bonn, Germany). Preparation procedures

Table 1. Nominal Starting Compositions (wt %) Used in the Present Study

Starting Composition	CaO	MgO	Al_2O_3	SiO_2	CO_2[a]
JADSCM-3	21.36	25.68	3.04	27.54	22.38
JADSCM-7	10.95	33.38	4.02	43.15	8.50
JADSCM-8	12.48	32.76	3.31	39.21	12.24
CMAS-CO_2-1	11.24	31.96	6.39	45.41	5.00
CMAS-CO_2-20	11.53	24.91	11.10	32.06	20.4
DN-1	15.10	29.49	7.02	37.69	10.70
DN-2	14.88	30.04	6.02	38.35	10.71
DN-8	9.96	30.88	14.96	35.09	9.11
DN-9	7.09	32.38	15.82	39.67	5.04
DN-10	19.33	24.41	11.93	29.07	15.26

[a]Added as magnesite, $MgCO_3$.

were identical to those reported in *Keshav and Gudfinnsson* [2013]. In brief, the silicate portion, consisting of glass, of the starting mixtures was prepared first in platinum (Pt) crucibles. In order to assure homogeneity, each silicate mixture was glassed twice. The silicate glass was reground for 1 h under ethanol in an agate mortar and then dried under an IR heat lamp for about 1 h. Finely ground magnesite (the source of some MgO and all of CO_2) was fired at 200–250 °C in air in a Pt crucible for over 17 h. Eventually, silicate and carbonate portion were mixed and ground in an agate mortar under ethanol for another 1 h and the final contents stored in a desiccator.

All the experiments reported here were performed in solid media devices at Bayerisches Geoinstitut (BGI, Bayreuth). Most of the experiments from 2 to 3 GPa were performed in a traditional, three-post piston-cylinder device with a maximum thrust of 250 t; some experiments at 3 GPa were performed also in a split-sphere multianvil apparatus that has a maximum thrust of 1200 t (Sumitomo 1200). Piston cylinder experiments employed ½″ (half-inch) talc-pyrex pressure cells. Multianvil experiments employed Cr_2O_3-doped MgO pressure cells with an edge length of 18 mm. Second-stage tungsten carbide (WC) anvils (32 mm edge length; Widia F grade) with 11 mm truncated edge lengths were employed in experiments performed at 3 GPa by means of multianvil apparatus. Pyrophyllite was used as gasket material in multianvil experiments and molybdenum (Mo) rings on either end of the stepped lanthanum chromite ($LaCrO_3$) heaters serve as electric contacts with the second-stage WC anvils.

The pressure cells used in the piston cylinder apparatus consist of stepped graphite heaters and soft MgO inserts. Pressure calibrations on the piston cylinder apparatus were done using the anorthite-spinel (forsterite + opx + cpx + anorthite + spinel + melt [*Presnall et al*., 1979]) and spinel-garnet (forsterite + opx + cpx + spinel + garnet + melt [*Milholland and Presnall*, 1998]) peridotite solidus transitions in the system CMAS. Using the device at BGI, we have located the anorthite-spinel and spinel-garnet peridotite solidus transitions at 0.94 GPa/1310 °C and 2.95 GPa/1585 °C, respectively, which are not far off from previously published experimental data. This close convergence of ideal pressures done with talc-pyrex (this study) and salt-pyrex [*Klemme and O'Neill*, 2000] pressure cells is encouraging. In situ multianvil experiments indicate that the spinel-garnet peridotite solidus transition in the system CMAS occurs at about 2.5–2.6 GPa [*Walter et al*., 2002]. More recently, *Longhi* [2005] experimentally located the spinel-garnet peridotite solidus transition at 2.9 GPa, which is again in very close agreement with *Milholland and Presnall* [1998] and pressure determinations reported here. The precision in pressure and temperature is estimated to be on the order of about 0.5 kbar and 10–12 °C, respectively. The reported experiments were performed using the *hot piston-out* method.

In the experiments performed using piston-cylinder device, the final (after the run) Pt capsule dimensions are at approximately 1.5 mm wide by 1.5 long; similarly, multianvil capsules are roughly 600 μm wide by 1 mm long. For all experiments (including those of pressure-temperature calibrations), ~0.5–0.8 mg of a starting mixture was loaded into a Pt capsule that had previously been annealed in air at 1000 °C, sealed at one end by arc welding, boiled in dilute HCl (30 mins), ultrasonically cleaned in ethanol (10 mins), and fired again in air at 1000 °C

Table 2. Select Run Conditions and Resulting Phase Assemblages[a]

Run	Starting Mixture	Pressure (GPa)	Temperature (°C)	Duration (h)	Phase Assemblage
B-373	DN-2	2	1425	6	fo + cpx + sp + glass + int.liq + vap?
B-260	CMAS-CO_2-20	2	1445	24	fo + cpx + sp + glass + int.liq + vap
B-375	DN-2	2	1470	6	fo + glass + vap
B-378	DN-2	2	1490	6	fo + glass + vap
B-372	DN-2	2.2	1435	6	fo + cpx + sp + glass + int.liq + vap
B-363	DN-2	2.2	1460	6	fo + cpx + sp + glass + int.liq
B-455	CMAS-CO_2-1	2.2	1460	6	fo + opx + cpx + sp + glass + int.liq
B-457	CMAS-CO_2-20	2.2	1460	6	fo + cpx + sp + glass + int.liq + vap
B-446	DN-8	2.2	1475	6	fo + cpx + sp + glass + int.liq + vap?
B-389	DN-2	2.2	1515	6	fo + glass + vap-?
B-379	DN-2	2.4	1425	6	fo + cpx + sp + glass + int.liq + vap
B-383	DN-2	2.4	1450	6	fo + cpx + sp + glass + int.liq + vap?
B-355	DN-2	2.4	1475	6	fo + cpx + sp + glass + int.liq + vap?
B-452	CMAS-CO_2-1	2.4	1475	6	fo + opx + cpx + sp + glass + int.liq
B-453	CMAS-CO_2-20	2.4	1475	6	fo + cpx + sp + glass + int.liq + vap?
B-659	DN-10	2.4	1475	6	fo + cpx + sp + glass + int.liq + vap?
B-445	DN-8	2.4	1500	6	fo + cpx + sp + glass + int.liq + vap?
B-306	CMAS-CO_2-1	2.4	1525	6	fo + opx + cpx + glass
B-351	DN-2	2.6	1400	6	fo + cpx + gt + glass + int.liq + vap
B-350	DN-2	2.6	1425	6	fo + cpx + gt + glass + int.liq + vap?
B-349	DN-1	2.6	1450	6	fo + cpx + gt + glass + int.liq
B-324	DN-1	2.6	1475	6	fo + cpx + gt + glass + int.liq
B-447	DN-9	2.6	1500	6	fo + cpx + sp + gt + glass + int.liq
B-308	CMAS-CO_2-1	2.6	1560	6	fo + opx + cpx + glass
B-384	DN-2	2.8	1325	6	fo + opx + cpx + gt + int.liq
B-288	JADSCM-8	2.8	1375	6	fo + opx + cpx + gt + int.liq
B-290	JADSCM-8	2.8	1425	6	fo + opx + cpx + int.liq
B-319	DN-1	2.8	1425	6	fo + cpx + gt + int.liq
B-291	JADSCM-7	2.8	1475	6	fo + opx + cpx + int.liq
B-318	DN-1	2.8	1475	6	fo + cpx + gt + int.liq
B-292	CMAS-CO_2-1	2.8	1525	6	fo + opx + cpx + sp + int.liq
B-450	CMAS-CO_2-1	2.8	1550	6	fo + opx + cpx + sp + int.liq
B-314	DN-1	2.8	1550	6	fo + glass
B-376	DN-2	3	1475	3	fo + opx + cpx + gt + int.liq
B-377	DN-2	3	1500	3	fo + opx + cpx + gt + int.liq

[a]fo, forsterite; opx, orthopyroxene; cpx, clinopyroxene; sp, spinel; gt, garnet; int.liq, interstitial liquid; and vap, vapor. Also see Tables 3 and 4.

for 10 mins. Before assembling the pressure cell, the loaded capsule was again dried in air at 175–200 °C for over 14 h. Run temperature was measured using type D ($W_{75}Re_{25}/W_{97}Re_3$) thermocouple wires (0.25 mm thick; Omega®). A 0.5 mm thick MgO disc (fired in air at 1000 °C for 1 h) separated the thermocouple junction from the capsule in piston cylinder experiments. In multianvil runs, the thermocouple wires were in direct contact with the Pt capsule. Dense, 4-bore alumina tubes (99.97% purity) were used to contain the thermocouple wires.

Temperatures reported in the manuscript are thermocouple readings. The effect of pressure on the thermocouple emf was ignored. Temperature was controlled to within ±1 °C of the target temperature using a Eurotherm controller. To ensure anhydrous conditions during the experiments, all the cell parts (except talc-pyrex pressure cells, graphite heaters, Mo electrodes, and capsules) were fired in air at 1000 °C in a box furnace for 1 h. After construction and before an experiment, the entire cell was kept dry in an oven at 175 °C. Each experiment was kept at its target pressure and temperature for 3 to 6 h, with only one exception where the run duration was about 1 day (Table 2). Experiments were quenched by turning off the power supply to the graphite and lanthanum chromite heaters, and decompression was carried out in approximately 10–15 min. Multianvil experiments were compressed to the desired pressure in about 3–4 h and, after the experiments, were decompressed to room pressure over 8–10 h.

After each run, the capsule was mounted longitudinally in epoxy and ground and polished for optical and electron microprobe examination. After termination of a multianvil experiment, the thermocouple junction was

Table 3. Experimental Details, Run Products, and Electron Microprobe Analyses (wt %) of Crystalline Phases and Quenched Melts/Liquids Away From the Carbonated Peridotite Solidus Ledge[a]

Run (P/T/Bulk)	CaO	MgO	Al_2O_3	SiO_2	CO_2	Sum
B-373 (2 GPa/1425 °C/DN-2)[b]						
fo (10)[c]	0.47 (0.04)[d]	55.14 (0.30)	0.20 (0.08)	41.90 (0.20)	98.70 (0.31)	
cpx (10)	22.24 (0.27)	17.39 (0.30)	9.26 (0.54)	50.44 (0.40)	99.32 (0.39)	
glass (11)	31.76 (1.00)	9.55 (1.71)	10.14 (0.76)	30.61 (1.78)	17.94 (1.50)[e]	100.00
int.liq. (11)	43.92 (3.20)	7.68 (2.30)	0.58 (0.58)	3.39 (2.39)	44.44 (2.65)	100.00
B-260 (2 GPa/1445 °C/CMAS-CO_2-20)						
fo (9)	0.44 (0.02)	57.17 (0.15)	0.25 (0.24)	43.10 (0.28)	100.96 (0.16)	
cpx (2)	18.48 (3.37)	19.81 (3.09)	12.33 (0.59)	48.48 (1.57)	99.09 (0.69)	
sp (2)	0.145 (0.01)	30.23 (2.75)	65.53 (6.42)	3.49 (4.41)	99.39 (0.73)	
glass (20)	21.27 (0.12)	19.50 (0.11)	11.36 (0.10)	39.01 (0.23)	8.86 (0.39)	100.00
int.liq. (20)	42.65 (1.97)	11.01 (1.39)	0.43 (0.34)	2.43 (1.61)	43.48 (1.76)	100.00
B-375 (2 GPa/1470 °C/DN-2)						
fo (15)	0.47 (0.03)	57.04 (0.37)	0.09 (0.02)	42.86 (0.24)	100.45 (0.55)	
glass (13)	20.56 (0.19)	21.02 (0.24)	8.89 (0.10)	41.01 (0.21)	8.52 (0.63)	100.00
B-378 (2 GPa/1490 °C/DN-2)						
fo (10)	0.43 (0.02)	56.91 (0.39)	0.11 (0.03)	42.63 (0.30)	100.08 (0.42)	
glass (12)	20.03 (1.94)	21.31 (3.09)	8.81 (0.61)	41.20 (0.23)	8.66 (0.94)	100.00
B-372 (2.2 GPa/1435 °C/DN-2)						
fo (8)	0.33 (0.03)	57.24 (0.23)	0.07 (0.01)	42.33 (0.24)	99.98 (0.41)	
cpx (11)	20.23 (0.45)	21.06 (1.20)	5.20 (2.50)	53.51 (1.48)	100.00 (0.36)	
glass (16)	19.46 (0.17)	21.62 (0.28)	8.66 (0.10)	39.81 (0.27)	10.44 (0.48)	100.00
int.liq. (28)	40.78 (2.74)	11.98 (2.29)	0.47 (0.63)	2.23 (2.17)	44.55 (2.53)	100.00
B-363 (2.2 GPa/1460 °C/DN-2)						
fo (13)	0.42 (0.04)	57.26 (0.16)	0.10 (0.04)	42.65 (0.19)	100.43 (0.27)	
cpx (12)	20.57 (0.48)	20.29 (1.27)	6.53 (3.11)	52.59 (2.06)	99.97 (0.55)	
glass (16)	20.44 (0.44)	21.05 (0.61)	8.90 (0.37)	40.95 (1.49)	8.67 (1.36)	100.00
int.liq. (4)	44.18 (0.89)	10.04 (1.73)	0.48 (0.19)	2.39 (0.87)	42.90 (0.82)	100.00
B-455 (2.2 GPa/1460 °C/CMAS-CO_2-1)						
fo (10)	0.35 (0.02)	57.46 (0.20)	0.10 (0.02)	42.47 (0.15)	100.38 (0.23)	
opx (10)	2.83 (0.08)	36.66 (0.45)	3.48 (0.97)	57.45 (0.60)	100.42 (0.20)	
cpx (11)	16.53 (0.84)	24.55 (0.79)	5.24 (0.57)	54.21 (0.57)	100.52 (0.30)	
glass (3)	21.61 (0.11)	10.27 (0.77)	13.97 (0.62)	48.34 (0.40)	5.81 (0.71)	100.00
int.liq (4)	38.33 (3.03)	13.47 (1.20)	1.47 (0.67)	2.43 (1.63)	44.31 (0.90)	100.00
B-457 (2.2 GPa/1460 °C/CMAS-CO_2-20)						
fo (11)	0.39 (0.04)	57.42 (0.18)	0.22 (0.13)	42.59 (0.19)	100.63 (0.25)	
cpx (9)	17.52 (0.73)	20.67 (0.56)	14.21 (0.57)	47.30 (0.44)	99.70 (0.18)	
sp (7)	0.13 (0.04)	28.19 (0.22)	70.61 (0.19)	0.41 (0.04)	99.34 (0.42)	
glass (9)	19.62 (0.17)	22.42 (0.19)	10.92 (0.29)	37.66 (0.17)	9.38 (0.51)	100.00
int.liq (7)	44.66 (1.16)	10.83 (1.88)	1.36 (1.06)	3.67 (2.23)	39.48 (2.02)	100.00
B-446 (2.2 GPa/1475 °C/DN-8)						
fo (8)	0.36 (0.03)	57.15 (0.16)	0.24 (0.07)	41.91 (0.24)	99.60 (0.31)	
cpx (9)	15.57 (3.07)	20.46 (2.93)	16.15 (0.83)	47.21 (1.00)	99.39 (0.53)	
sp (9)	0.11 (0.02)	27.89 (0.34)	71.29 (0.50)	0.35 (0.02)	99.65 (0.80)	
glass (15)	21.13 (0.65)	10.43 (0.86)	17.15 (0.53)	43.16 (0.49)	8.13 (0.60)	100.00
int.liq (4)	41.89 (2.66)	13.26 (2.10)	1.00 (0.88)	2.91 (1.67)	40.95 (1.44)	100.00
B-389 (2.2 GPa/1515 °C/DN-2)						
fo (11)	0.41 (0.02)	57.61 (0.15)	0.11 (0.01)	42.92 (0.18)	101.05 (0.23)	
glass (12)	19.08 (0.25)	24.10 (0.56)	8.30 (0.08)	40.92 (0.10)	7.61 (0.34)	100.00
B-379 (2.4 GPa/1425 °C/DN-2)						
fo (7)	0.32 (0.03)	56.88 (0.38)	0.13 (0.02)	42.46 (0.18)	99.78 (0.43)	
cpx (11)	20.35 (0.13)	19.47 (0.26)	8.52 (0.69)	51.56 (0.39)	99.85 (0.25)	
glass (15)	29.37 (2.53)	11.89 (3.51)	9.62 (1.40)	29.27 (3.12)	19.85 (3.55)	100.00
int.liq. (22)	40.88 (2.75)	11.27 (1.84)	0.74 (0.66)	2.70 (1.81)	44.41 (2.40)	100.00
B-383 (2.4 GPa/1450 °C/DN-2)						
fo (10)	0.38 (0.03)	57.49 (0.17)	0.15 (0.06)	42.96 (0.19)	100.98 (0.20)	
cpx (13)	20.44 (0.20)	20.11 (0.32)	7.53 (0.78)	52.30 (0.57)	100.39 (0.35)	
glass (12)	20.78 (0.77)	20.93 (1.36)	9.22 (0.31)	38.57 (0.31)	10.51 (0.63)	100.00
int.liq (19)	41.62 (2.28)	11.53 (1.34)	0.51 (0.37)	1.48 (0.81)	44.86 (1.81)	100.00

Table 3. (continued)

Run (P/T/Bulk)	CaO	MgO	Al_2O_3	SiO_2	CO_2	Sum
B-355 (2.4 GPa/1475 °C/DN-2)						
fo (5)	0.42 (0.08)	56.36 (0.32)	0.12 (0.05)	42.87 (0.40)	99.77 (0.38)	
cpx (1)	16.68	22.89	7.06	53.32	99.95	
glass (30)	19.39 (0.10)	22.38 (0.15)	8.45 (0.06)	40.76 (0.20)	9.02 (0.23)	100.00
int.liq. (2)	42.30 (5.37)	11.54 (2.94)	0.67 (0.55)	2.89 (3.40)	42.61 (1.51)	100.00
B-452 (2.4 GPa/1475 °C/CMAS-CO_2-1)						
fo (10)	0.35 (0.02)	56.89 (0.22)	0.11 (0.02)	41.85 (0.29)	99.19 (0.42)	
opx (10)	2.84 (0.10)	36.13 (0.25)	3.67 (0.85)	56.77 (0.56)	99.41 (0.24)	
cpx (10)	18.22 (2.50)	20.42 (4.05)	10.32 (4.77)	50.10 (3.64)	99.05 (0.77)	
glass (10)	18.10 (1.79)	19.81 (3.11)	10.49 (0.81)	45.07 (0.81)	6.52 (0.73)	100.00
int.liq (17)	39.03 (2.13)	14.15 (1.98)	0.68 (0.65)	1.90 (1.75)	44.23 (2.41)	100.00
B-453 (2.4 GPa/1475 °C/CMAS-CO_2-20)						
fo (8)	0.35 (0.03)	56.58 (0.38)	0.28 (0.25)	41.78 (0.21)	98.99 (0.37)	
cpx (8)	16.55 (1.24)	20.19 (1.26)	14.82 (0.69)	46.43 (0.67)	97.98 (0.68)	
sp (10)	0.09 (0.04)	27.65 (0.18)	71.26 (0.38)	0.37 (0.03)	99.37 (0.55)	
glass (14)	18.21 (0.54)	22.30 (0.46)	11.56 (0.49)	37.91 (1.10)	10.01 (1.59)	100.00
int.liq (8)	40.12 (3.16)	13.60 (2.20)	0.85 (0.81)	2.83 (2.17)	42.60 (2.14)	100.00
B-659 (2.4 GPa/1475 °C/DN-10)						
fo (8)	0.44 (0.02)	56.81 (0.17)	0.39 (0.22)	41.71 (0.48)	99.36 (0.23)	
cpx (9)	18.22 (0.76)	20.27 (0.52)	12.38 (0.70)	47.31 (0.33)	98.18 (0.28)	
sp (11)	0.12 (0.03)	28.73 (0.21)	69.97 (0.28)	0.43 (0.13)	99.24 (0.25)	
glass (10)	21.55 (0.28)	17.67 (0.59)	8.01 (0.29)	32.76 (0.15)	20.00 (1.03)	100.00
int.liq (17)	33.26 (3.71)	20.69 (3.45)	1.31 (0.67)	14.06 (3.49)	30.70 (3.50)	100.00
B-445 (2.4 GPa/1500 °C/DN-8)						
fo (10)	0.34 (0.03)	56.93 (0.16)	0.32 (0.22)	41.47 (0.25)	99.06 (0.30)	
cpx (7)	14.10 (0.83)	21.99 (0.63)	16.00 (0.34)	46.95 (0.44)	99.04 (0.68)	
sp (10)	0.10 (0.02)	27.87 (0.22)	71.15 (0.43)	0.40 (0.02)	99.53 (0.60)	
glass (9)	20.16 (0.74)	11.72 (0.78)	16.57 (0.49)	42.73 (0.60)	8.82 (0.56)	100.00
int.liq (11)	43.10 (1.10)	12.37 (0.99)	0.37 (0.39)	1.06 (1.06)	43.10 (1.43)	100.00
B-306 (2.4 GPa/1525 °C/CMAS-CO_2-1)						
fo (10)	0.33 (0.03)	56.73 (0.15)	0.10 (0.02)	42.09 (0.16)	99.25 (0.28)	
opx (10)	2.92 (2.27)	36.28 (2.40)	3.36 (1.62)	57.18 (1.46)	99.74 (0.35)	
cpx (13)	16.83 (0.12)	20.86 (0.16)	11.22 (0.39)	50.04 (0.38)	98.96 (0.20)	
glass (78)	15.78 (0.24)	23.37 (0.19)	8.95 (0.08)	45.37 (0.33)	6.53 (0.34)	100.00
B-351 (2.6 GPa/1400 °C/DN-2)						
fo (12)	0.42 (0.36)	57.20 (0.71)	0.21 (0.19)	42.89 (0.25)	100.72 (0.39)	
cpx (9)	20.20 (0.63)	19.78 (0.60)	9.16 (0.97)	50.77 (1.33)	99.91 (0.70)	
glass (8)	24.25 (1.60)	16.20 (3.14)	9.42 (1.12)	33.12 (4.68)	17.02 (7.2)	100.00
int.liq. (2)	41.25 (2.62)	11.63 (1.65)	0.35 (0.24)	1.01 (0.25)	45.77 (0.50)	100.00
B-350 (2.6 GPa/1425 °C/DN-2)						
fo (10)	0.35 (0.03)	57.19 (0.41)	0.19 (0.15)	42.64 (0.33)	100.36 (0.60)	
cpx (7)	20.34 (0.40)	19.56 (0.69)	8.94 (0.74)	50.76 (1.33)	99.60 (0.88)	
gt (11)	6.90 (3.29)	31.44 (11.08)	17.83 (8.02)	44.18 (1.52)	100.36 (1.05)	
glass (25)	24.68 (2.80)	18.51 (2.05)	7.74 (0.90)	31.07 (3.41)	18.00 (3.01)	100.00
int.liq. (5)	39.23 (3.64)	14.77 (4.52)	0.90 (0.69)	6.17 (2.71)	38.92 (3.29)	100.00
B-349 (2.6 GPa/1450 °C/DN-1)						
fo (14)	0.39 (0.13)	57.03 (0.31)	0.21 (0.11)	42.58 (0.23)	100.20 (0.38)	
cpx (15)	19.05 (0.81)	20.47 (0.78)	9.12 (2.58)	51.69 (1.43)	100.33 (0.32)	
gt (20)	7.25 (0.23)	24.27 (0.21)	25.32 (0.14)	44.19 (0.25)	101.04 (0.37)	
glass (31)	20.02 (0.17)	21.28 (0.15)	9.81 (0.08)	36.87 (0.22)	12.02 (0.27)	100.00
int.liq. (22)	42.31 (2.03)	12.05 (0.83)	0.66 (0.53)	2.21 (1.66)	42.77 (0.89)	100.00
B-324 (2.6 GPa/1475 °C/DN-1)						
fo (8)	0.37 (0.04)	56.86 (0.15)	0.20 (0.08)	42.49 (0.26)	99.93 (0.39)	
cpx (10)	18.99 (0.91)	19.87 (0.47)	10.26 (1.65)	50.35 (1.07)	99.46 (0.40)	
gt (10)	7.75 (0.40)	24.25 (0.28)	24.22 (0.90)	44.28 (0.41)	100.51 (0.32)	
glass (30)	20.18 (0.23)	20.84 (0.34)	9.82 (0.09)	36.61 (0.13)	12.55 (0.25)	100.00
int.liq. (12)	41.06 (2.21)	11.76 (1.78)	0.34 (0.39)	2.15 (1.65)	44.70 (1.27)	100.00
B-447 (2.6 GPa/1500 °C/DN-9)						
fo (10)	0.24 (0.04)	57.26 (0.59)	0.69 (1.45)	41.72 (0.60)	99.90 (0.55)	

Table 3. (continued)

Run (P/T/Bulk)	CaO	MgO	Al_2O_3	SiO_2	CO_2	Sum
cpx (8)	11.86 (2.06)	22.98 (2.09)	16.76 (0.55)	47.54 (0.34)	99.12 (0.38)	
sp (10)	0.08 (0.03)	28.00 (0.16)	71.34 (0.28)	0.47 (0.05)	99.89 (0.35)	
gt (10)	5.29 (0.23)	26.31 (0.19)	25.25 (0.17)	43.98 (0.22)	100.83 (0.23)	
glass (11)	18.17 (1.14)	10.95 (1.69)	15.01 (2.94)	43.86 (0.64)	12.01 (2.28)	100.00
int.liq (10)	35.91 (4.84)	16.29 (1.58)	1.68 (2.14)	2.70 (2.60)	43.42 (1.48)	100.00
B-308 (2.6 GPa/1560 °C/CMAS-CO_2-1)						
fo (10)	0.31 (0.06)	56.77 (0.33)	0.13 (0.07)	42.16 (0.30)	99.37 (0.35)	
opx (10)	2.40 (0.19)	36.78 (0.40)	2.74 (0.37)	57.76 (0.32)	99.68 (0.29)	
cpx (15)	17.96 (2.05)	19.76 (2.35)	11.11 (1.81)	49.78 (1.90)	98.61 (0.74)	
glass (30)	14.24 (0.10)	25.24 (0.15)	8.36 (0.09)	45.46 (0.19)	6.69 (0.28)	100.00
B-384 (2.8 GPa/1325 °C/DN-2)						
fo (10)	0.27 (0.05)	57.56 (0.32)	0.12 (0.09)	42.92 (0.32)	100.86 (0.43)	
opx (10)	2.35 (0.22)	35.70 (0.75)	8.16 (2.02)	54.52 (1.35)	100.72 (0.38)	
cpx (12)	19.94 (0.28)	21.88 (0.34)	4.32 (0.57)	54.01 (0.42)	100.14 (0.37)	
gt (10)	6.69 (1.23)	25.43 (0.60)	24.66 (1.66)	44.42 (0.68)	101.20 (0.51)	
int.liq (18)	38.20 (2.88)	14.60 (1.80)	0.24 (0.16)	3.26 (1.90)	43.70 (1.96)	100.00
B-288 (2.8 GPa/1375 °C/JADSCM-8)						
fo (10)	0.25 (0.03)	57.10 (0.15)	0.10 (0.04)	42.90 (0.27)	100.35 (0.29)	
opx (10)	2.14 (0.15)	36.16 (0.22)	5.68 (0.49)	56.32 (0.42)	100.30 (0.26)	
cpx (10)	18.70 (0.46)	22.30 (0.46)	5.12 (0.83)	53.63 (0.34)	99.76 (0.40)	
gt (10)	6.41 (0.29)	25.37 (0.30)	24.62 (0.84)	44.56 (0.39)	100.97 (0.46)	
int.liq. (8)	39.52 (2.50)	14.44 (0.92)	0.25 (0.26)	2.44 (2.58)	43.36 (2.80)	100.00
B-290 (2.8 GPa/1425 °C/JADSCM-8)						
fo (10)	0.32 (0.04)	56.62 (0.31)	0.13 (0.09)	42.84 (0.31)	99.91 (0.25)	
opx (10)	2.54 (0.13)	35.94 (0.32)	4.90 (0.47)	56.60 (0.17)	99.98 (0.35)	
cpx (10)	15.94 (0.27)	24.36 (0.41)	5.01 (0.65)	54.23 (0.50)	99.54 (0.17)	
int.liq. (9)	37.41 (2.04)	13.67 (0.80)	0.76 (0.62)	3.55 (1.95)	44.61 (1.80)	100.00
B-319 (2.8 GPa/1425 °C/DN-1)						
fo (10)	0.31 (0.05)	57.04 (0.65)	0.57 (1.34)	42.21 (0.73)	100.13 (0.45)	
cpx (10)	18.77 (0.18)	22.27 (0.26)	4.44 (0.34)	53.72 (0.35)	99.19 (0.48)	
gt (4)	8.15 (1.14)	25.25 (1.02)	22.22 (1.78)	44.73 (0.83)	100.34 (0.30)	
int.liq. (6)	38.89 (0.83)	14.11 (0.51)	0.18 (0.17)	1.13 (1.28)	45.70 (0.56)	100.00
B-291 (2.8 GPa/1475 °C/JADSCM-7)						
fo (10)	0.24 (0.03)	57.51 (0.13)	0.06 (0.01)	42.81 (0.23)	100.62 (0.25)	
opx (10)	2.58 (0.30)	36.97 (0.28)	3.28 (0.72)	57.54 (0.41)	100.37 (0.28)	
cpx (10)	15.93 (1.38)	23.78 (1.35)	7.16 (0.48)	52.96 (0.44)	99.84 (0.33)	
int.liq. (41)	41.26 (2.16)	13.43 (1.51)	0.17 (0.25)	0.51 (0.66)	44.62 (1.28)	100.00
B-318 (2.8 GPa/1475 °C/DN-1)						
fo (10)	0.32 (0.03)	57.15 (0.21)	0.27 (0.41)	42.48 (0.29)	100.23 (0.14)	
cpx (10)	17.79 (0.21)	22.65 (0.23)	5.88 (0.53)	53.33 (0.35)	99.65 (0.39)	
gt (4)	6.71 (1.21)	25.07 (0.47)	24.66 (1.23)	44.41 (0.39)	100.85 (0.27)	
int.liq. (10)	39.35 (1.48)	13.38 (0.72)	0.28 (0.25)	1.20 (0.93)	45.79 (0.57)	100.00
B-292 (2.8 GPa/1525 °C/CMAS-CO_2-1)						
fo (10)	0.30 (0.03)	57.44 (0.18)	0.13 (0.02)	42.75 (0.21)	100.63 (0.26)	
opx (10)	2.72 (0.06)	36.24 (0.37)	4.74 (0.68)	56.41 (0.50)	100.21 (0.32)	
cpx (10)	13.60 (1.24)	25.33 (1.82)	8.23 (3.34)	52.36 (2.14)	99.51 (0.44)	
sp (1)	0.07	30.66	65.49	3.81	100.04	
int.liq. (23)	39.37 (2.69)	14.50 (1.91)	0.12 (0.13)	0.93 (1.20)	45.09 (1.46)	100.00
B-450 (2.8 GPa/1550 °C/CMAS-CO_2-1)						
fo (10)	0.31 (0.02)	57.09 (0.21)	0.12 (0.04)	42.06 (0.15)	99.58 (0.29)	
opx (11)	2.80 (0.27)	36.59 (0.36)	3.42 (0.73)	57.21 (0.59)	100.02 (0.37)	
cpx (10)	18.18 (1.76)	19.88 (1.85)	11.52 (1.72)	49.95 (1.36)	99.53 (0.41)	
int.liq (9)	39.91 (1.99)	14.29 (1.11)	0.60 (0.53)	1.89 (1.83)	43.31 (1.91)	100.00
B-314 (2.8 GPa/1550 °C/DN-1)						
fo (10)	0.32 (0.02)	57.10 (0.14)	0.14 (0.02)	42.67 (0.20)	100.23 (0.24)	
glass (20)	17.27 (0.11)	24.46 (0.09)	8.29 (0.05)	38.49 (0.16)	11.49 (0.21)	100.00
B-376 (3 GPa/1475 °C/DN-2)						
fo (12)	0.34 (0.04)	57.03 (0.38)	0.17 (0.15)	42.52 (0.22)	100.06 (0.22)	
opx (9)	2.93 (0.52)	35.74 (0.75)	6.35 (1.28)	55.34 (1.63)	100.36 (0.54)	

Table 3. (continued)

Run (P/T/Bulk)	CaO	MgO	Al_2O_3	SiO_2	CO_2	Sum
cpx (7)	16.75 (0.66)	23.84 (0.46)	5.45 (1.00)	53.65 (1.01)	99.70 (0.61)	
gt (7)	6.47 (0.94)	26.42 (0.62)	23.19 (1.63)	45.22 (0.58)	101.29 (0.37)	
int.liq. (7)	39.04 (2.94)	13.39 (2.59)	0.89 (0.54)	3.67 (2.41)	43.01 (2.36)	100.00
B-377 (3 GPa/1500 °C/DN-2)						
fo (10)	0.32 (0.04)	57.30 (0.33)	0.12 (0.02)	42.77 (0.25)	100.51 (0.46)	
opx (6)	2.79 (0.24)	35.74 (0.35)	5.80 (0.87)	56.05 (0.92)	100.38 (0.40)	
cpx (12)	16.32 (0.38)	24.38 (0.70)	5.41 (0.89)	54.11 (0.96)	100.22 (0.48)	
gt (7)	6.56 (0.82)	25.52 (0.65)	24.80 (0.20)	44.86 (0.17)	101.74 (0.12)	
int.liq. (16)	40.15 (2.21)	13.60 (0.97)	0.49 (0.46)	1.38 (1.13)	44.40 (1.59)	100.00

[a]Also note Tables 2 and 4. In many runs in this table, spinel is present but its composition not provided. Hence, the runs here should be read together with those in Table 2. Details are fo, forsterite; opx, orthopyroxene; cpx, clinopyroxene; sp, spinel; gt, garnet; int.liq, interstitial liquid; glass, silicate melt; and int.liq., carbonatitic melt.
[b]In parentheses: pressure (P) in GPa, temperature (T) in degree Celsius, and starting composition (bulk).
[c]Number of analyses.
[d]Number in parentheses is the standard deviation.
[e]The amount of CO_2 is calculated by difference, and its standard deviation is based on this amount.

Table 4. Experimental Details, Run Products, and Electron Microprobe Analyses (wt.%) of Crystalline Phases and Quenched Melts Defining the Carbonated Peridotite Solidus Ledge[+++]

Run	CaO	MgO	Al_2O_3	SiO_2	CO_2	Sum	Ca#[++]
1 (JADSCM-3)[%]							
3.0 GPa/1225°C/6 hours							
Forsterite (12)*	0.25 (0.04)	57.50 (0.12)	0.06 (0.03)	42.75 (0.2)		100.56	
Opx (13)	2.70 (0.24)	36.23 (0.17)	4.50 (0.23)	57.10 (0.30)		100.53	
Cpx (15)[$]	21.20 (0.86)	23.01 (0.75)	5.53 (0.23)	51.10 (0.21)		100.84	
Garnet (10)	7.01 (0.19)	25.14 (0.29)	24.37 (0.39)	43.51 (0.29)		100.03	
Mag-Cal (10)	40.38 (0.59)	14.17 (0.37)			45.45[+]	100.00	67.05
Melt (30)	36.93 (1.31)	15.59 (1.07)	0.23 (0.07)	3.13 (0.93)	44.12	100.00	62.85
19 (JADSCM-3)[#]							
2.9 GPa/1225°C/6 hours							
Forsterite (9)	0.39 (0.19)	56.93 (0.52)	0.21 (0.06)	41.79 (0.61)		99.32	
Opx (17)	2.56 (0.31)	35.77 (0.39)	5.03 (0.21)	57.22 (0.77)		100.58	
Garnet (9)	7.21 (0.35)	24.83 (0.79)	24.61 (0.61)	43.24 (0.49)		99.89	
Mag-Cal (13)	41.80 (0.33)	13.69 (0.55)			44.51	100.00	68.56
Melt (25)	38.26 (1.55)	18.34 (1.11)	0.16 (0.08)	5.51 (1.79)	37.73	100.00	59.84
2 (JADSCM-3)[#]							
2.8 GPa/1275°C/6 hours							
Forsterite (15)	0.15 (0.09)	56.50 (0.23)	0.06 (0.04)	42.75 (0.29)		99.46	
Opx (16)	2.52 (0.31)	36.01 (0.26)	4.59 (0.21)	56.92 (0.39)		100.04	
Cpx (12)	20.03 (0.93)	22.98 (0.95)	5.01 (0.27)	51.10 (0.39)		99.12	
Garnet (11)	9.09 (0.29)	23.31 (0.66)	24.15 (0.43)	43.49 (0.38)		100.04	
Melt (30)	36.81 (1.17)	15.68 (1.01)	0.20 (0.07)	3.09 (0.73)	44.22	100.00	62.64
13 (JADSCM-3)							
2.8 GPa/1250°C/6 hours							
Forsterite (8)	0.19 (0.05)	57.1 (0.19)	0.27 (0.09)	42.53 (0.31)		100.09	
Cpx (17)	19.93 (0.47)	23.72 (0.51)	5.19 (0.41)	52.14 (0.69)		100.98	
Garnet (9)	8.59 (0.88)	24.68 (0.61)	23.83 (0.37)	43.18 (0.54)		100.28	
Melt (15)	37.41 (0.97)	17.92 (1.11)	0.39 (0.17)	4.57 (1.77)	39.71	100.00	59.85
3 (JADSCM-3)							
2.7 GPa/1325°C/6 hours							
Forsterite (16)	0.33 (0.09)	57.01 (0.20)	0.08 (0.03)	42.11 (0.30)		99.53	
Opx (11)	2.01 (0.17)	35.98 (0.31)	5.53 (0.30)	56.50 (0.41)		100.02	
Cpx (14)	19.99 (0.72)	19.50 (0.95)	7.97 (0.31)	52.50 (0.44)		99.96	
Garnet (11)	5.50 (0.23)	25.51 (0.70)	24.48 (0.51)	45.01 (0.44)		100.50	
Melt (30)	37.51 (0.79)	16.02 (0.86)	0.41 (0.10)	0.51 (0.30)	45.55	100.00	62.60

Table 4. (continued)

Run	CaO	MgO	Al_2O_3	SiO_2	CO_2	Sum	$Ca\#^{++}$
12 (JADSCM-3)#							
2.7 GPa/1310°C/6 hours							
Forsterite (6)	0.29 (0.07)	57.13 (0.42)	0.22 (0.09)	42.61 (0.28)		100.25	
Cpx (18)	20.33 (0.71)	20.92 (0.59)	8.11 (0.88)	51.37 (0.64)		100.73	
Garnet (10)	6.19 (0.22)	25.38 (0.35)	24.31 (0.79)	44.79 (0.93)		100.67	
Melt (19)	36.18 (1.23)	17.62 (2.06)	0.37 (0.19)	4.49 (1.79)	41.34	100.00	59.45
17 (JADSCM-3)#							
2.7 GPa/1225°C/6 hours							
Forsterite (11)	0.34 (0.13)	56.71 (0.32)	0.16 (0.08)	42.76 (0.44)		99.97	
Opx (13)	2.36 (0.22)	36.11 (0.47)	5.81 (0.26)	56.27 (0.57)		100.55	
Cpx (19)	20.83 (0.85)	21.01 (1.05)	7.87 (0.49)	51.17 (0.57)		100.88	
Melt (30)	37.06 (0.93)	16.23 (0.79)	0.18 (0.13)	7.51 (2.33)	39.02	100.00	61.99
4 (CMAS-CO_2-1)#							
2.6 GPa/1370°C/6 hours							
Forsterite (12)	0.21 (0.06)	55.99 (0.32)	0.07 (0.02)	42.99 (0.28)		99.26	
Opx (12)	2.03 (0.10)	36.03 (0.40)	5.50 (0.26)	57.10 (0.51)		100.66	
Cpx (10)	20.06 (0.66)	19.10 (0.81)	8.90 (0.20)	51.97 (0.51)		100.03	
Garnet (10)	4.99 (0.19)	26.01 (0.91)	24.20 (0.60)	45.51 (0.52)		100.71	
Melt (31)	37.99 (0.90)	15.10 (0.81)	0.4 (0.13)	1.10 (0.56)	45.41	100.00	64.40
11 (CMAS-CO_2-1)							
2.6 GPa/1350°C/6 hours							
Forsterite (10)	0.34 (0.08)	56.24 (0.29)	0.11 (0.04)	42.59 (0.36)		99.28	
Cpx (14)	21.1 (0.72)	19.14 (0.63)	8.23 (0.88)	50.96 (0.49)		99.43	
Garnet (6)	5.33 (0.76)	25.86 (0.29)	24.3 (0.33)	44.79 (0.51)		100.28	
Melt (13)	35.81 (0.88)	18.10 (1.06)	0.41 (0.19)	4.20 (1.17)	41.48	100.00	58.56
5 (CMAS-CO_2-1)#							
2.4 GPa/1385°C/6 hours							
Forsterite (15)	0.20 (0.08)	57.01 (0.29)	0.19 (0.09)	42.01 (0.31)		99.41	
Opx (10)	2.10 (0.17)	35.94 (0.38)	6.51 (0.59)	56.01 (0.60)		100.56	
Cpx (11)	18.01 (0.45)	22.91 (0.88)	6.10 (0.31)	53.51 (0.69)		100.53	
Garnet (9)	6.50 (0.31)	24.53 (0.90)	23.96 (0.73)	44.10 (0.61)		99.09	
Melt (20)	37.10 (0.80)	17.43 (0.91)	0.50 (0.19)	1.51 (0.61)	43.46	100.00	60.85
10 (CMAS-CO_2-1)#							
2.4 GPa/1380°C/6 hours							
Forsterite (12)	0.27 (0.12)	56.79 (0.29)	0.21 (0.08)	42.16 (0.44)		99.43	
Cpx (16)	18.27 (0.49)	23.09 (0.33)	6.34 (0.93)	53.12 (0.79)		100.82	
Garnet (5)	6.92 (0.38)	23.87 (0.0.26)	24.12 (0.19)	44.37 (0.51)		99.28	
Melt (9)	36.73 (0.1.73)	17.1 (2.19)	0.39 (0.17)	3.69 (1.67)	42.09	100.00	60.54
6 (CMAS-CO_2-1)#							
2.3 GPa/1395°C/6 hours							
Forsterite (15)	0.40 (0.11)	57.10 (0.36)	0.11 (0.04)	42.10 (0.39)		99.71	
Opx (10)	2.30 (0.23)	35.50 (0.44)	7.49 (0.64)	54.97 (0.71)		100.26	
Cpx (13)	18.11 (0.51)	23.10 (0.79)	7.53 (0.41)	52.07 (0.74)		100.81	
Garnet (5)	6.99 (0.40)	25.11 (0.87)	23.02 (0.80)	44.08 (0.72)		99.20	
Melt (25)	39.10 (0.91)	16.43 (0.88)	0.11 (0.02)	1.04 (0.61)	43.32	100.00	62.85
9 (CMAS-CO_2-1)#							
2.3 GPa/1390°C/6 hours							
Forsterite (9)	0.38 (0.11)	56.21 (0.53)	0.27 (0.09)	42.64 (0.39)		99.50	
Cpx (10)	18.21 (0.83)	22.83 (0.71)	7.67 (0.44)	51.58 (0.31)		100.29	
Garnet (7)	7.13 (0.29)	25.31 (0.17)	24.07 (0.21)	43.73 (0.38)		100.24	
Melt (19)	37.89 (1.26)	16.58 (1.89)	0.17 (0.07)	5.12 (1.64)	40.24	100.00	62.01
7 (CMAS-CO_2-1)#							
2.1 GPa/1410°C/6 hours							
Forsterite (12)	0.31 (0.10)	56.95 (0.43)	0.16 (0.08)	42.09 (0.46)		99.51	
Opx (10)	2.20 (0.21)	36.18 (0.45)	6.59 (0.73)	55.51 (0.64)		100.48	
Cpx (11)	17.50 (0.42)	22.11 (0.91)	8.06 (0.40)	51.57 (0.59)		99.24	
Spinel (6)	0.10 (0.06)	33.50 (0.61)	65.10 (0.59)	1.51 (0.89)		100.21	
Melt (20)	37.94 (0.91)	16.10 (0.73)	0.13 (0.05)	3.09 (0.98)	43.74	100.00	63.00
8 (CMAS-CO2-1)#							
2.1 GPa/1400°C/6 hours							
Forsterite (8)	0.26 (0.12)	55.89 (0.43)	0.19 (0.08)	43.04 (0.37)		99.38	
Cpx (11)	17.79 (0.59)	21.63 (0.83)	7.53 (0.71)	52.11 (0.89)		99.06	

Table 4. (continued)

Run	CaO	MgO	Al_2O_3	SiO_2	CO_2	Sum	Ca#[++]
Spinel (2)	0.07 (0.05)	34.27 (0.67)	66.41 (0.29)	1.24 (0.58)		101.99	
Melt (11)	38.12 (0.96)	15.31 (1.39)	0.22 (0.17)	4.23 (2.03)	42.12	100.00	63.99

[+++]Vapor is assumed to be pure CO_2.
[++]Ca# (Ca/Ca+Mg*100) in molar units.
[%]In parentheses is the starting composition used.
[#]Presence of vapor in these experiments was confirmed by piercing open Pt-capsules in ethanol.
*The number of analyses.
[$]Cpx-clinopyroxene, Opx-orthopyroxene, and Mag-Cal-magnesian calcite.
[+]CO_2 in magnesian calcite and melt calculated by difference.

confirmed to be always in direct contact with the capsule. The runs were polished under water-absent conditions, and charges also had to be vacuum impregnated multiple times with resin. High-temperature (1200–1600 °C) calibrations for the multianvil pressure cells employed in this study are derived on the basis of previous determinations done on Sumitomo 1200 at BGI (a review can be found in *Keppler and Frost* [2005]).

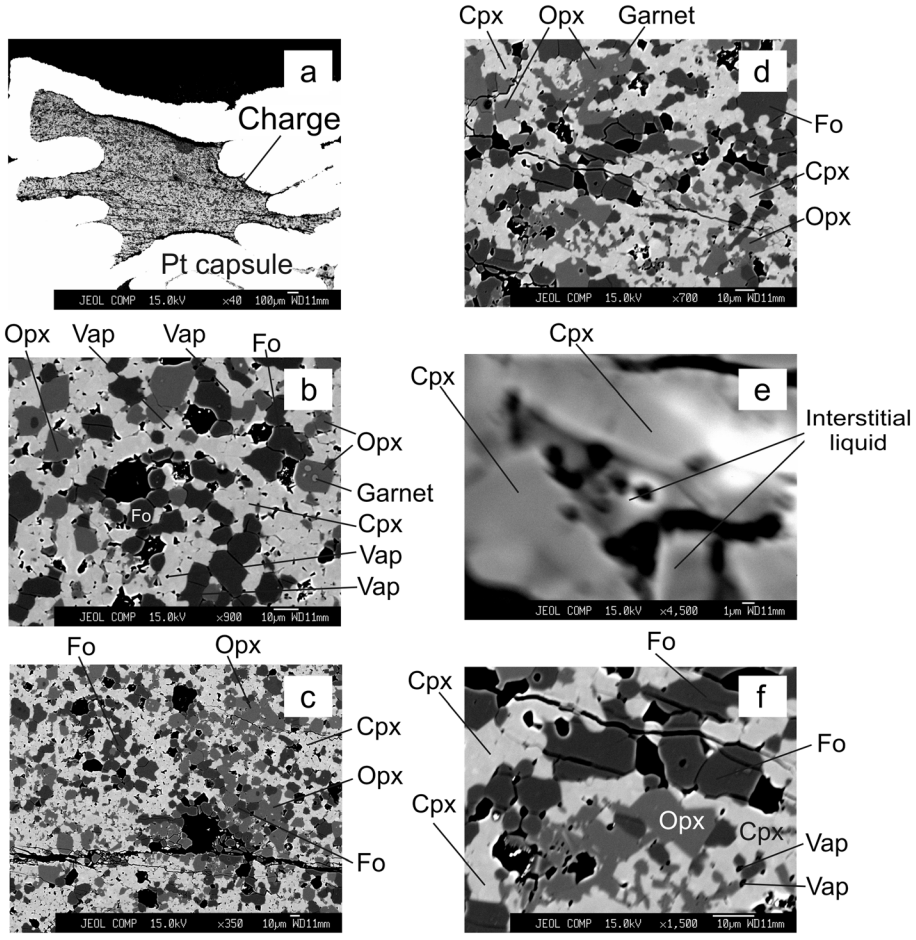

Figure 2. (a–f) Backscattered electron images of an experimental charge at 2.3 GPa and 1395 °C (run 6 in Table 4). This charge contains forsterite (fo), orthopyroxene (opx), clinopyroxene (cpx), garnet, CO_2 vapor (vap), and melt (quenched melt). Bright object in Figure 2a is Pt capsule. Presence of six phases in this run makes it isobarically invariant.

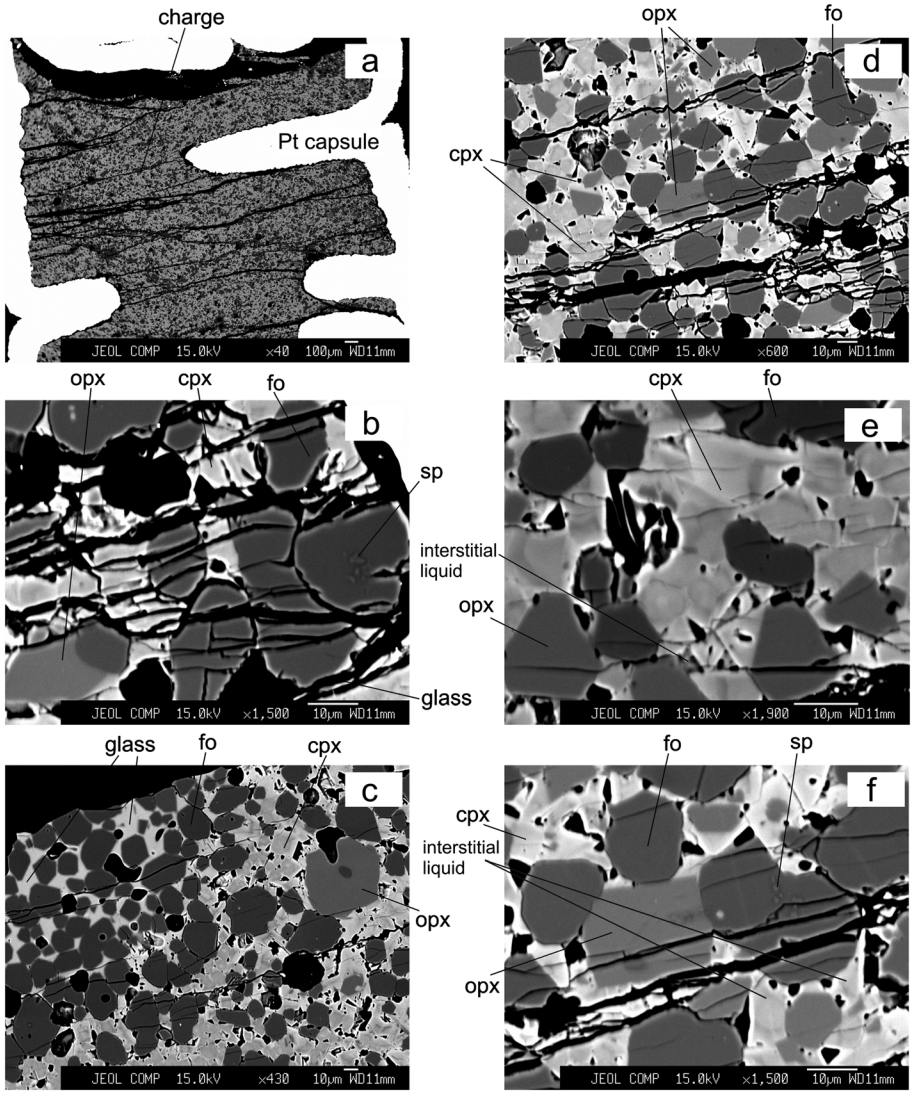

Figure 3. Backscattered electron images of the experimental charge B-455 at 2.2 GPa and 1460 °C (Table 2). In this run, peridotite crystalline phase assemblage of forsterite, orthopyroxene (opx), clinopyroxene (cpx), and spinel (sp) is found with interstitial liquid (carbonatite) and glass (silicate melt). These phase relations are isobarically invariant and indicate the presence of a univariant line in P-T space originating from an invariant point on the CMAS-CO_2 solidus involving forsterite + opx + cpx + spinel + vapor + carbonatite melt + silicate melt [see *Keshav and Gudfinnsson*, 2013]. This also puts constraints on the position of the transition line along which a spinel-peridotite phase assemblage changes to a garnet-peridotite one as being at a higher pressure than 2.2 GPa along the 1460 °C isotherm.

Compositions of the crystalline phases and melt were determined by wavelength-dispersive electron microprobe analyzer (5 spectrometer JEOL-JXA-8200 Superprobe at BGI) with an accelerating voltage of 15 kV and 15 nA probe current (at the Faraday cup). Melt was analyzed using a beam diameter of 1–5 μm. The beam diameter was 1–2 μm for crystalline phases, and all the analyses were performed in a fixed spot mode. Analyses were reduced using the ZAF correction scheme, and the amount of CO_2 in melt and crystalline carbonate was calculated by difference. Concentrations of all four oxides in the charges were measured using a combination of forsterite, diopside, pyrope, and enstatite standards.

3. Textures of Phases in the Experimental Charges

List of experiments and chemical composition of phases in this study are reported in Tables 2–4. To establish the presence of free vapor, some capsules were sliced open while immersed in a beaker containing ethanol, and bubbles were seen to escape from capsules toward the top of the beaker (Table 4). Experimental charges

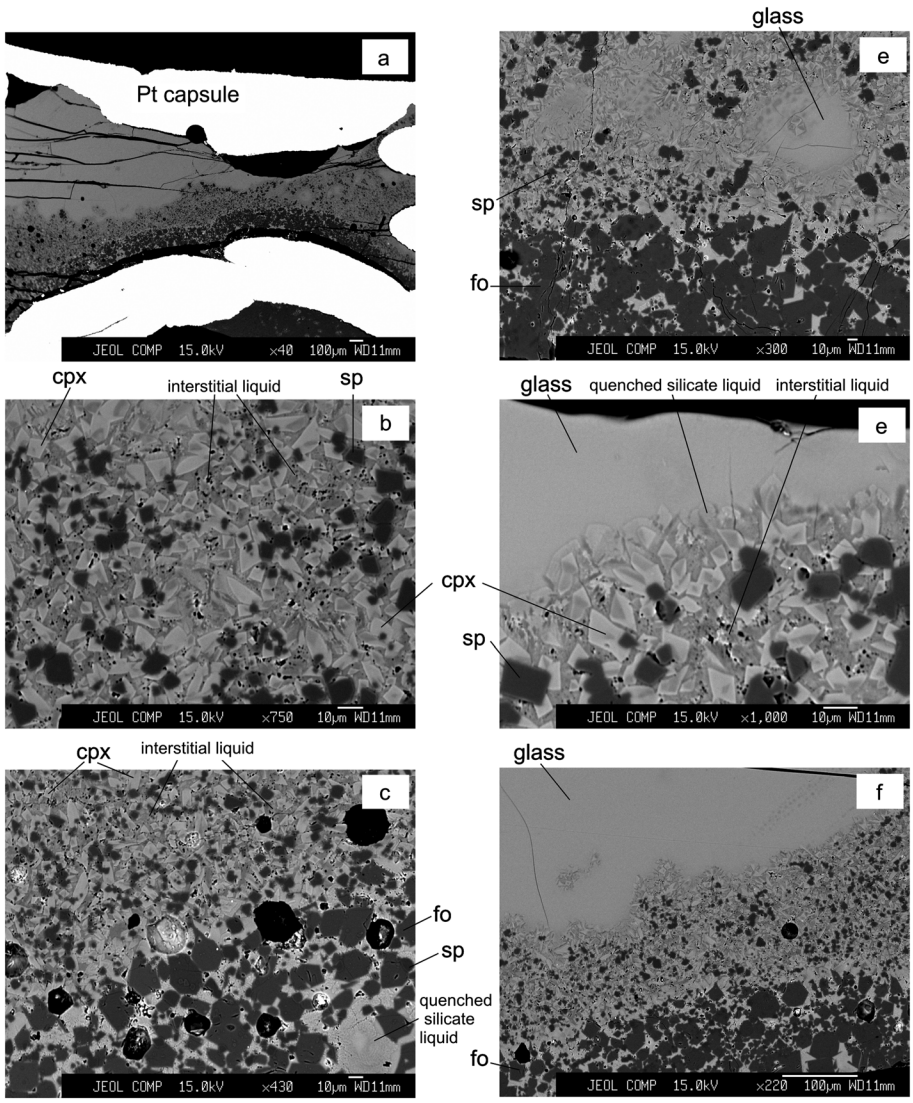

Figure 4. Backscattered electron images of experiment B-659 at 2.4 GPa and 1475 °C (Table 2). In this experiment, forsterite, clinopyroxene (cpx), spinel (sp) and vapor are in equilibrium with interstital liquid (carbonatite) and glass (silicate liquid or quenched silicate liquid).

that define the position of the solidus ledge are identified in Table 4. Backscattered electron images of a select few experimental charges are shown in Figures 2–4. Where possible, the composition of spinel is reported (Table 4), and in other cases, it is assumed to be stoichiometric, end-member composition ($MgAl_2O_4$). In experiment labeled B-351 (Table 2), due to the very small size of garnet, its reliable chemical composition could not be determined and therefore is not reported in Table 3.

At a given contrast and brightness, forsterite (fo) is the darkest crystalline phase (Figures 2–4). It is euhedral in outline, is about 10–15 μm across, and occurs uniformly throughout the charge. Normally, forsterite does not occur as an inclusion in any other crystalline phase but at places hosts small (~5–7 μm across) grains of garnet (gt) or spinel (sp). When present, opx is uniformly distributed throughout the charge (although see later), is about 10 μm across, and has a characteristic prismatic habit (Figures 2 and 3). Also like forsterite, opx hosts small, round grains of garnet (Figure 2b). For a given set of conditions, subhedral clinopyroxene (cpx) is the brightest crystalline silicate phase (Figures 2–4). Among silicate phases, garnet has the highest relief and can easily be distinguished from other phases owing to its roughly round habit (Figure 2b). To establish that the

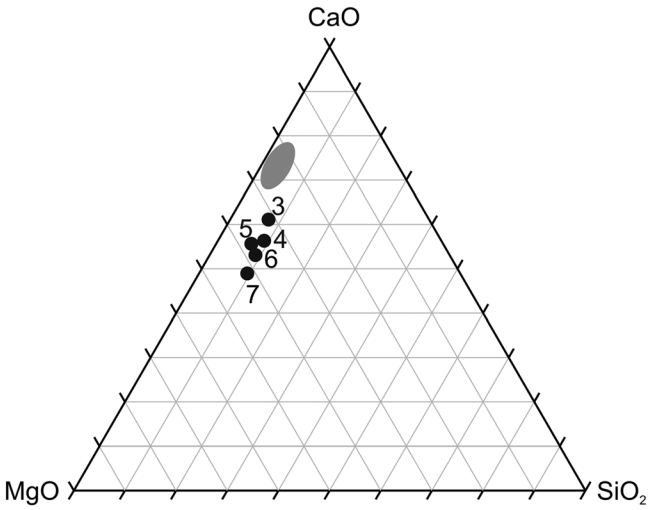

Figure 5. Projected from CO_2 onto the CaO-MgO-SiO_2 (CMS) base, this ternary (wt %) shows the locus of liquid compositions (in grey) along the carbonated peridotite solidus ledge as determined in the present study. Shown also are the liquid compositions (in solid circles) at the solidus of model carbonated in the system CMAS-CO_2 from *Dalton and Presnall* [1998]. Numbers adjacent to these solid circles are pressure in gigapascal (GPa). Note that melts in the system CMAS-CO_2 (present study and *Dalton and Presnall* [1998]), because they have a very small amount of alumina, are slightly off this plane.

obtained results are reproducible within uncertainty, experiments at 2.3 GPa/1425 °C and 2.8 GPa/1275 °C were repeated and resulted in identical findings to initial experiments.

Crystalline carbonate (magnesian calcite, described later) is light grey, frequently occupies low-lying areas, is fractured, has a slight perforated appearance, and hosts discrete grains of opx and garnet. Crystalline carbonate in this work occurs in two experimental charges: 2.9 GPa/1225 °C and 3 GPa/1225 °C, performed in piston cylinder and multianvil apparatus, respectively. Spinel often occurs as inclusions hosted in forsterite grains (Figures 3 and 4) and generally does not exceed 2–8 μm across.

All the experimental charges are porous, features we interpret to have developed in the presence of free CO_2 vapor. It is because of this porosity that charges had to be vacuum impregnated at least 4–5 times. Vapor (Figures 2–4) dominantly occurs as oblate and rather rotund bodies latching onto the boundaries of other phases. At places, vapor attains almost roundish outlines but can also be elliptical and in this sense resembles the textures described in *Watson and Brenan* [1987] and *Brenan and Watson* [1988]. Vapor reported in the experiments to some extent also resembles the one in liquid-bearing experiments in *Hammouda* [2003].

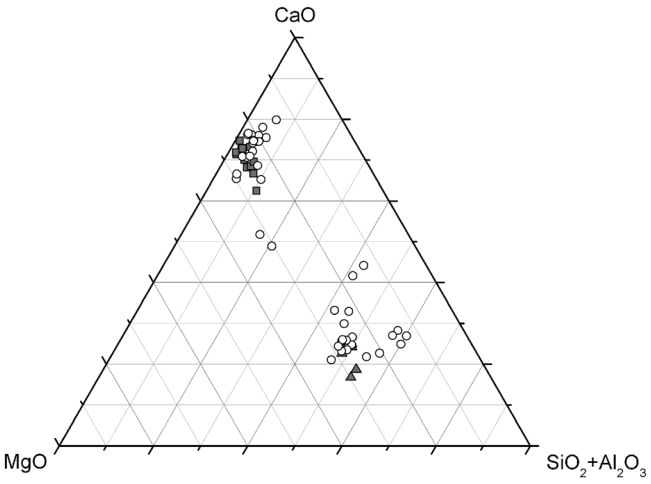

Figure 6. Projected from CO_2 and displayed in this ternary CaO-MgO-SiO_2 [(+Al_2O_3), CMS + A] are liquid compositions from experiments away from the solidus ledge (see Figures 7 and 9). Filled, grey triangles are silicate melts as the *only* liquid with one of more crystalline phase(s) and/or vapor (see Table 2). Filled, grey squares are only carbonatitic melts found in equilibrium with crystalline phases (see Table 2). Carbonatitic (close to the CaO apex) and silicate melts (close to the $SiO_2 + Al_2O_3$ apex) occurring in the *same* charge are both shown in blank circles (see Table 2).

Two texturally different melts are present in the experiment charges. The first kind of melt occurs only interstitially with individual melt pockets being approximately 3–10 μm across; this interstitial melt has a homogeneous distribution in the crystalline matrix. At 3 and 2.8 GPa, this interstitial melt coexists with forsterite, opx, cpx, and garnet. At P-T conditions corresponding to the solidus ledge (see later), only interstitial melt was observed in the crystalline matrix. The second type of melt occurs over 2–2.8 GPa and at temperatures higher than that of the ledge (see later). This second melt (Figures 3 and 4) tends to form relatively large, segregated bulbous pools, with a glassy and clear appearance.

In polished sections, the interstitial liquid and the clear segregated liquid (silicate in composition, described

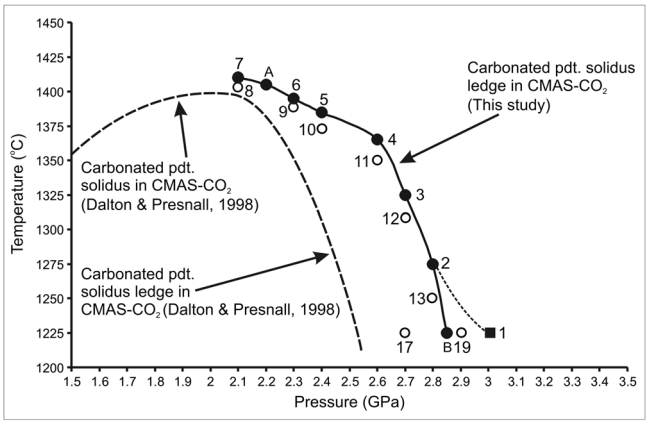

Figure 7. This temperature-pressure projection shows the experimentally determined melting phase relations along the solidus ledge from the present study (shown as a continuous curve connecting filled circles). Experimental runs labeled 2, 3, 4, 5, 6, and 7 (Table 4) have six phases (including liquid) and thus constitute isobaric invariant points. Runs labeled 8, 9, 10, 11, 12, 13, and 17 (Table 4), shown in blank circles, are on the lower temperature-pressure side of the solidus ledge, and are all liquid-bearing (liquid is found here because the starting mixtures were designed to have liquid in all experimental charges). Run labeled 19 (blank circle; Table 4) is an isobaric invariant point at 2.9 GPa/1225 °C consisting of forsterite-opx-garnet-vapor-magnesian calcite-melt. Point B at about 2.85 GPa/1225 °C is an inferred P-T invariant point whose identity is constrained by two runs, labeled 17 (2.7 GPa/1225 °C; forsterite-opx-cpx-vapor-melt; Table 4) and 19 (2.9 GPa/1225 °C; forsterite-opx-garnet-vapor-magnesian calcite-melt; Table 4). Therefore, point B should consist of forsterite-opx-cpx-garnet-vapor-magnesian calcite-liquid. Likewise, runs labeled 7 at 2.1 GPa/1410 and 6 at 2.3 GPa/1395 °C are two isobaric invariant points where the assemblage forsterite-opx-cpx-spinel-vapor-melt and forsterite-opx-cpx-garnet-vapor-melt respectively, are present. Thus, these two runs bracket yet another P-T invariant point, labeled A, which for now placed at 2.2 GPa/1405 °C, should have the assemblage forsterite-opx-cpx-spinel-garnet-vapor-melt. Therefore, given these data, the P-T univariant solidus ledge intersects two P-T invariant points A and B. Run labeled 1 (Table 4) at 3 GPa/1225 °C, the only one from multianvil apparatus, consists of forsterite-opx-cpx-garnet-vapor-magnesian calcite-melt, and is hence the only experiment containing a true P-T invariant assemblage. On the basis of runs 17, 19, 1, and point B, there are two solidus trajectories shown in this projection: joining of run 2 with B results in a solidus topology that is very similar to the one originally drawn in *Dalton and Presnall* [1998], while connecting run 2 with run 1, gives a topology which has a fair slope in this part of the solidus ledge. Also shown is the carbonated peridotite (pdt.) solidus construct from *Dalton and Presnall* [1998].

later) are not in physical contact with each other. These two melts are in general separated by crystalline (or quenched crystalline) phases or glass that is composed of quenched components. On this basis, it could be suggested that one possible consequence of these quench crystals is to produce the interstitial liquid (carbonatitic in composition; see the next section) by enriching the residual carbonate component of a prequench, silicate melt. As to why this cannot be the case, and also as to why observations presented here are reproducible, and hence are tantamount to being real features in the experimental charges, is discussed at some length in the companion study [*Keshav and Gudfinnsson*, 2013].

4. Compositions of Liquids in the Experimental Charges

The interstitial liquid, in equilibrium with model peridotite phase assemblage, is a model carbonatite in composition, with Ca# (molar Ca/Ca + Mg*100) of ~58–66 (Figures 5 and 6 and Tables 3 and 4).

The second melt is silicate in composition with some dissolved CO_2 and is much less calcic than its counterpart (exceptions are runs labeled B-373 and B-379; Table 3). This silicate melt is first observed at 2.8 GPa at 1550 °C. Interstitial and segregated liquids that have model carbonatite and silicate compositions, respectively, occur together over a fairly narrow pressure-temperature interval of 2 to 2.6 GPa and 1425 to 1500 °C (Tables 2 and 3). Chemical compositions of carbonatitic and silicate melts, when found together, are shown in Figure 6.

5. The Solidus Ledge of Carbonated Peridotite in the System CMAS-CO_2

In the present study, the solidus of model carbonated peridotite, defining the ledge, is as follows: (1) 2.1 GPa and 1410 °C - forsterite + opx + cpx + spinel + vapor + melt; (2) 2.3 GPa/1395 °C, 2.4 GPa/1385 °C, 2.6 GPa/1370 °C, 2.7 GPa/1325 °C, and 2.8 GPa/1275 °C - forsterite + opx + cpx + garnet + vapor + melt; and (3) 2.85 GPa and 1225 °C - forsterite + opx + cpx + garnet + vapor + magnesian calcite + melt.

With six phases present from 2.1 to 2.8 GPa, melting phase relations are isobarically invariant, making the solidus ledge P-T univariant, and along the ledge as shown in Figure 7, there is only *one* liquid (labeled "melt" in the reactions above) that occurs interstitially. Compared with previous constructs (Figure 1, this study, taken from *Dalton and Presnall* [1998] and *Gudfinnsson and Presnall* [2005]), the experimentally determined

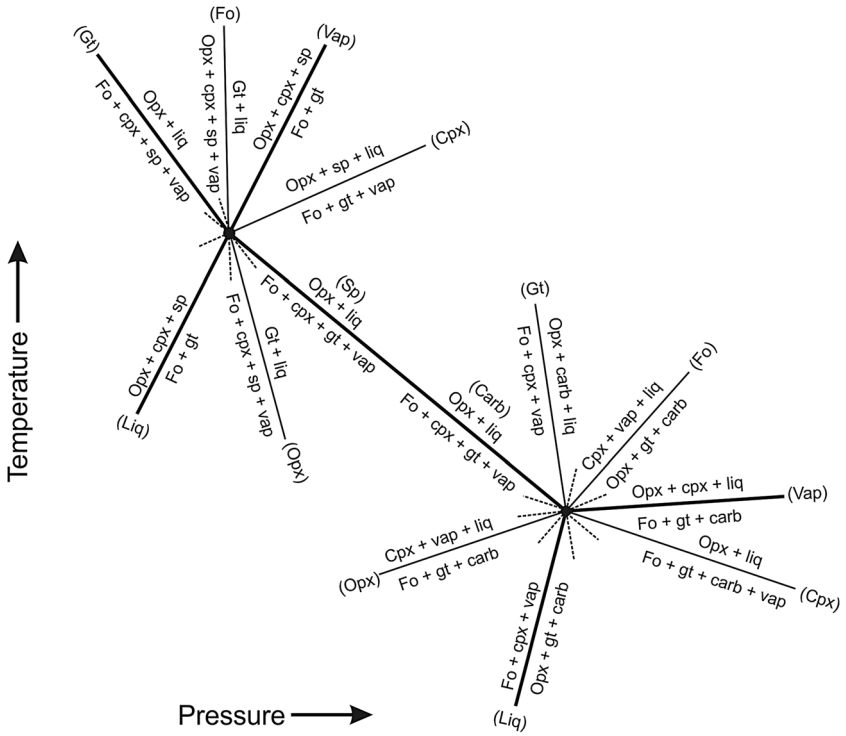

Figure 8. Schreinemakers' construct showing melting of model, vapor-bearing carbonated peridotite between 2.1 and 3 GPa. This construct shows what the solidus of model carbonated peridotite would look like at the (left) spinel-garnet and (right) vapor-crystalline carbonate transitions. Phases in parentheses label the univariant curves according to the absent phase. Phases labeled carb and liq, either in parentheses or otherwise, are crystalline carbonate and carbonatitic liquid, respectively. The P-T univariant lines of most significance are shown in bold and further discussion on this construct is in the part "Reactions along the solidus ledge" in the manuscript.

carbonate ledge (Figure 7) is somewhat displaced toward higher temperatures and higher pressures in P-T space. The experimentally determined curve based on *piston cylinder* experiments, except for being slightly more open at low pressures than previous constructs, maintains the overall shape found in previous studies. The lowest part of the ledge is defined by two runs at 2.7 GPa (forsterite + opx + cpx + vapor + liquid; run "17" shown as an open circle in Figure 7) and 2.9 GPa (forsterite + opx + garnet + vapor + magnesian calcite + liquid; run "19" shown as an open circle in Figure 7) at 1225 °C. Therefore, these two runs constrain a P-T invariant point that is required to have the assemblage forsterite + opx + cpx + garnet + vapor + magnesian calcite + liquid. In Figure 7, this P-T invariant point, marked as "B" (filled circle), is placed at 2.85 GPa and 1225 °C. However, when the sole run made in the *multianvil* at 3 GPa/1225 °C (shown as filled square labeled "1" in Figure 7) containing a P-T invariant assemblage forsterite + opx + cpx + garnet + vapor + magnesian calcite + liquid is considered, the lowest part of the ledge would have more curvature (shown as dashed curve, connecting runs "2" and "1" in Figure 7). In all likelihood, the difference in the two topologies shown is due to the differences in the pressure calibration between the two devices.

Melt compositions along the ledge, or on either side of it, remain carbonatitic with about 38–44 wt % dissolved CO_2 (Tables 3 and 4 and Figures 5 and 6). Previously, the compositions of liquids in the system CMS-CO_2 along the ledge have been debated [*Eggler*, 1975, 1976; *Eggler et al*., 1976; *Wyllie and Huang*, 1976a, 1976b] (also briefly reviewed in *Luth* [1999, 2006]). For instance, *Eggler* [1976] and *Eggler et al*. [1976] suggested that in the system CMS-CO_2, the liquid in equilibrium with peridotite mineral assemblage at 3 GPa had about 20 wt % CO_2, and that the liquid between 2.6 and 3 GPa is broadly "kimberlitic" in composition, not "carbonatitic". From investigations in the systems MgO-SiO_2-CO_2 and CMS-CO_2, *Wyllie and Huang* [1975, 1976a, 1976b] suggested that melt in equilibrium with model peridotite, vapor, and crystalline carbonate at approximately 3 GPa had ~40 wt % CO_2. Hence, such liquids are carbonatitic in composition;

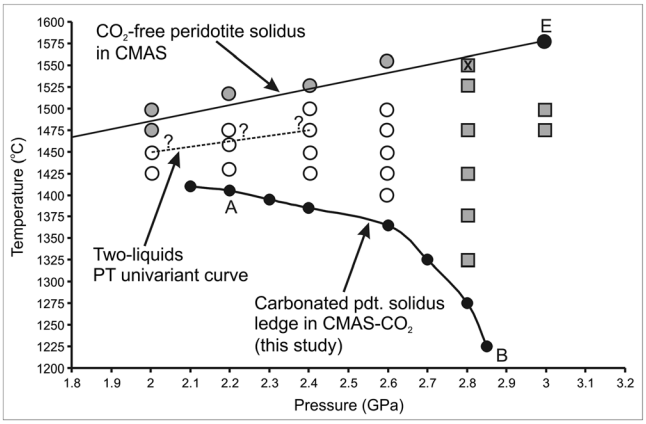

Figure 9. Temperature-pressure diagram showing experimentally determined solidus curves of dry and carbonated peridotite in the systems CMAS and CMAS-CO_2, labeled "CO_2-free peridotite solidus in CMAS" and "Carbonated pdt. solidus ledge in CMAS-CO_2", respectively. The solidus of model peridotite in the system CMAS is after *Presnall et al*. [1979], *Gudfinnsson and Presnall* [1996], *Milholland and Presnall* [1998], and *Liu and Presnall* [2000]. The solidus ledge as determined in the present study in the system CMAS-CO_2 is between point B and the pressure datum of 2.1 GPa. The P-T invariant points B and A are discussed under "Reactions along the solidus ledge" in the manuscript; point "E" is a P-T invariant point on the solidus of model peridotite in the system CMAS and consists of the assemblage forsterite + opx + cpx + spinel + garnet + melt [*Milholland and Presnall*, 1998]. The two-liquids line/curve, where we infer the existence of the assemblage forsterite + opx + cpx + spinel + carbonatitic liquid + silicate liquid, will be P-T univariant, and exists on the P-T divariant surface between the solidus ledge from the present study and the dry solidus of model peridotite in CMAS. The position of this two-melt line on the mentioned P-T divariant region is not precisely known (but according to the data presented in this study, should exist), and is therefore, shown as dashed line with question marks. The cross-in-grey square at 2.8 GPa and 1550 °C is where we deduce, on the basis of two runs, B-450 and B-314 (Table 2), using starting compositions CMAS-CO_2-1 and DN-1, respectively, carbonatitic liquid to silicate liquid transition. Symbols represent the following: filled, grey squares = carbonatitic melt; filled, grey circles = only silicate melt; blank circles = experiments containing both carbonatitic and silicate melt.

while only at pressure of 2.7–2.8 GPa, melt is found to be broadly "basaltic" in composition. Such *immediate* high CO_2 in the liquid was ascribed to carbonation-decarbonation reactions [*Wyllie and Huang*, 1976a, 1976b; *Wyllie*, 1987a, 1987b]. In *Eggler et al*. [1976], it is also clearly stated that the solubility of CO_2 vapor in various liquids in the system CMS-CO_2 increases regularly, rather than abruptly, as Wyllie and coworkers suggested. Eggler and coworkers and Wyllie and coworkers did not have alumina in the system they studied (CMS-CO_2). Hence, it is possible that the addition of alumina to CMS-CO_2 (as in this work) causes liquids to become carbonatitic not at 3 GPa but at 2.1 GPa.

Notwithstanding this early debate, the experimental work of *Gudfinnsson and Presnall* [2005] indicates that the major oxide isopleths are such so as to suggest an expanding area wherein carbonatites are produced with decreasing pressure down to at least 3 GPa. Hence, the liquid compositions presented here (Tables 3 and 4) along and in the vicinity of the ledge confirm that the P-T divariant region of carbonatite generation in the system CMAS-CO_2 [*Gudfinnsson and Presnall*, 2005] continues down to at least 2 GPa (Figure 7) [see also *Keshav and Gudfinnsson*, 2013].

At this point we compare compositions of crystalline carbonate and the coexisting liquid in light of the pseudo-binary $CaCO_3$-$MgCO_3$ at 1 [*Byrnes and Wyllie*, 1981], 2.7 [*Irving and Wyllie*, 1975], and 6 GPa [*Buob et al*., 2006]. As a function of pressure, the Ca# of minimum melt composition in the pseudo-binary $CaCO_3$-$MgCO_3$ turns increasingly magnesian from approximately 68 (1 GPa), 58–59 (2.7 GPa), and finally to 49 (6 GPa). The composition of the liquid (Ca# ~60; Table 4) at the P-T invariant point (Figure 7) bracketed using two *piston cylinder* runs at 2.7–2.9 GPa/1225 °C is in fair agreement with the composition of the minimum melt on the carbonate pseudo-binary at 2.7 GPa [*Irving and Wyllie*, 1975]. On the other hand, the Ca# (~63) of the liquid at the P-T invariant point from the *multianvil* run at 3 GPa/1225 °C is not only slightly higher than from piston cylinder runs but is also higher than the minimum melt composition on the carbonate join at 2.7 GPa [*Irving and Wyllie*, 1975]. This observation likely reflects differences in pressure calibrations between the piston cylinder and multianvil devices coupled with strongly pressure dependent changes in compositions. However, the temperature (1225 °C) of the P-T invariant point at 2.8–3 GPa compares well with the minimum melting temperature (~1235 °C; with some extrapolation from 2.7 to 3 GPa in *Irving and Wyllie* [1975]) [see *Buob et al*., 2006] on the carbonate join. Such close correspondence suggests that crystalline carbonate, at least at these P-T conditions, dominates the liquid composition and melting temperatures on the complex carbonate-silicate join in the mantle composition space (also see *Hammouda* [2003]).

6. Reactions Along the Solidus Ledge of Carbonated Peridotite in the System CMAS-CO_2

The experimental data (Table 4) have been used to evaluate melting reactions (wt %) along the carbonated peridotite solidus ledge, adopting the approach outlined in *Presnall* [1986]. The uncertainties in these reactions are roughly of the same magnitude as in the phase compositions. The calculated melting reactions are as follows:

2.1 GPa:

$$1.45\ fo + 2.53\ cpx + 0.03\ sp + 0.42\ CO_2 = 3.43\ opx + 1.00\ liq$$

2.3 GPa:

$$1.43\ fo + 2.44\ cpx + 0.42\ gt + 0.43\ CO_2 = 3.75\ opx + 1.00\ liq$$

2.4 GPa:

$$1.47\ fo + 2.33\ cpx + 0.40\ gt + 0.44\ CO_2 = 3.63\ opx + 1.00\ liq$$

2.6 GPa:

$$1.36\ fo + 2.20\ cpx + 0.19\ gt + 0.45\ CO_2 = 3.18\ opx + 1.00\ liq$$

2.7 GPa:

$$1.41\ fo + 2.16\ cpx + 0.12\ gt + 0.45\ CO_2 = 3.14\ opx + 1.00\ liq$$

2.8 GPa:

$$1.25\ fo + 2.45\ cpx + 0.10\ gt + 0.46\ CO_2 = 3.23\ opx + 1.00\ liq$$

In the reactions, the abbreviations correspond to the following: fo = forsterite, opx = orthopyroxene, cpx = clinopyroxene, sp = spinel, gt = garnet, CO_2 = vapor, and liq = carbonatitic liquid. All the solidus ledge reactions are of peritectic type, with opx being produced upon melting. The amount of opx in these reactions does not show much variation and as vapor provides all the CO_2 for the melt to make it carbonatitic and the amount of CO_2 in the melt does not make dramatic excursions, the contribution of vapor in the melting reactions is nearly constant. The calcic nature of melts is acquired from cpx, and the reaction coefficients for cpx are also similar across the pressure range.

Experiments at 2.1, 2.3, and 2.8–3 GPa are of particular interest. At 2.1 and 2.3 GPa the experimental charges contain two different isobarically invariant phase assemblages (Table 4); on this basis, there must be a P-T invariant point at approximately 2.2 GPa/1405 °C consisting of forsterite + opx + cpx + spinel + garnet + vapor + liquid, marking the transition from vapor-bearing spinel peridotite to vapor-bearing garnet peridotite (named "A" in Figure 7); there exists compositional degeneracy at A, making liquid and vapor co-planar. Another invariant point is identified at 2.85 GPa/1225 °C (Table 4), which consists of forsterite + opx + cpx + garnet + vapor + magnesian calcite + liquid (named B in Figure 7).

From the data in Table 4, the relative positions of all the P-T univariant curves that emanate from these two P-T invariant points have been calculated. With the particular phase-absent reaction marked in parentheses, the reactions are as follows:

2.2 GPa/1405 °C:

(Fo) $0.12\ opx + 2.03\ cpx + 0.65\ sp + 0.22\ vapor = 2.54\ gt + 0.48\ liq$

(Opx) $0.12\ fo + 5.01\ cpx + 1.55\ sp + 0.56\ vapor = 6.01\ gt + 1.23\ liq$

(Cpx) $2.03\ fo + 4.25\ gt + 0.22\ vapor = 5.01\ opx + 0.99\ spinel + 0.50\ liq$

(Sp) $0.65\ fo + 0.99\ cpx + 0.12\ gt + 0.18\ vapor = 1.53\ opx + 0.41\ liq$

(Gt) $2.53\ fo + 4.24\ cpx + 0.12\ sp + 0.74\ vapor = 6.01\ opx + 1.62\ liq$

(Vap) (Liq) $0.50\ fo + 1.67\ gt = 1.27\ opx + 0.50\ cpx + 0.40\ sp$

2.85 GPa/1225 °C:

(Fo) $4.15\ opx + 0.35\ gt + 7.63\ carb = 4.82\ cpx + 0.90\ vapor + 6.41\ liq$

(Opx) $0.41\ fo + 0.096\ gt + 1.81\ carb = 0.40\ cpx + 0.05\ vapor + 1.87\ liq$

(Cpx) $0.48\ fo + 0.07\ gt + 0.02\ carb + 1.37\ vapor = 0.40\ opx + 1.54\ liq$

(Gt) $3.55\ fo + 7.84\ cpx + 1.62\ vapor = 9.65\ opx + 2.26\ carb + 1.10\ liq$

(Vap) $0.90\ fo + 0.16\ gt + 2.90\ carb = 0.56\ opx + 0.20\ cpx + 3.20\ liq$

(Carb) $0.76\ fo + 1.37\ cpx + 0.02\ gt + 0.29\ vapor = 1.79\ opx + 0.65\ liq$

(Liq) $0.64\ fo + 1.56\ cpx + 0.32\ vapor = 1.87\ opx + 0.01\ gt + 0.64\ carb$

In the first set, the reactions of interest are spinel absent (Sp), garnet absent (Gt), and liquid absent (and by extension, vapor absent (Vap)). The composition of the liquid (Liq) in the written reactions is carbonatitic; and carb (Carb) is crystalline carbonate. Geometrical constructs of these two invariant points are shown in Figure 8. The construct displaying the spinel-garnet transition (corresponding to point A in Figure 1) in carbonated peridotite, shown in Figure 8 (left), is consistent with the presence of a small cusp (that is not experimentally resolvable) on the solidus. At pressures greater or lower than (Sp) or (Gt), reaction coefficients do not change much along these two P-T univariant curves. Similarly, in the second set, the reactions of interest are vapor absent (Vap), crystalline carbonate absent (Carb), and liquid absent (Liq). In the absence of experimental data, *Dalton and Presnall* [1998] inferred reaction coefficients at the vapor-carbonate transition at 2.6 GPa in the system CMAS-CO_2, which allows us to compare the reactions produced here experimentally at 2.85 GPa/1225 °C; in the present study vapor-carbonate P-T invariant point is shown in Figure 8 (right) (corresponding to point "B" in Figure 1). For example, along (Fo), *Dalton and Presnall* [1998] have vapor, opx, and dolomite reacting to produce cpx, garnet, and liquid, while in our case opx, garnet, and carbonate react to generate cpx, vapor, and liquid. The coefficients for garnet being produced along (Opx) and (Cpx) in *Dalton and Presnall* [1998] are very small, and if taken at face value, vapor, cpx, forsterite, and carbonate react to produce garnet and liquid, and vapor, opx, forsterite, and carbonate react to produce garnet and liquid, along (Opx) and (Cpx), respectively; but since the coefficients for garnet in (Opx) and (Cpx) are small, the possibility that garnet could just as well exist on the reactant side cannot be discounted.

The isobarically invariant melting reactions and their coefficients over 2.1–2.8 GPa written here are very similar to those for carbonate-absent (Carb) reaction in *Dalton and Presnall* [1998]. Yet for the reaction (Vap) deduced from experimental data set in the present study, opx and cpx are in reaction relation with the liquid, at the expense of forsterite, garnet, and magnesian calcite. On the other hand, at the 3 GPa isobaric invariant point in *Dalton and Presnall* [1998] (experimental work), opx is a reactant, along with dolomite and garnet, and produces forsterite and cpx upon melting. Hence, if the constructs and experiments are correctly interpreted, opx and forsterite along the (Vap) P-T univariant curve in the present study and isobaric invariance at 3 GPa in *Dalton and Presnall* [1998] change sides, leading to perhaps another singularity between 2.85 and 3 GPa.

The reaction (Gt) of Figure 8 terminates at point "C" in Figure 1, and according to this construct (Figure 1), liquid at point "C" is "basaltic". On the other hand, the reaction (Sp) of Figure 8 terminates at point B (Figure 1), and our results show that the liquid is carbonatitic in composition. Reaction (Carb) terminates at point "A" in Figure 1, while reaction (Vap) terminates at point "F" in Figure 1. The reactions at points A and B in Figure 7 and point "F" in Figure 1 produce carbonatitic melts according to the present experimental data, implying that carbonatite-to-silicate melt transition along the solidus of model, vapor-bearing peridotite occurs at some pressure lower than 2.1 GPa; this possibility has been confirmed experimentally in the companion study [*Keshav and Gudfinnsson*, 2013]. Therefore, in the present study, melting along the carbonated peridotite solidus ledge involves a reaction where carbonatitic melt is produced from reaction of CO_2 vapor and silicates.

7. Unmixing Between Carbonatitic and Silicate Melt

In the present study at 3 GPa and 1500 °C, liquid, in equilibrium with forsterite + opx + cpx + garnet, is carbonatitic (Tables 2 and 3). At 2.8 GPa, carbonatite melts are produced over the temperature interval of 1325–1550 °C (Table 3). However, in an experiment at 1550 °C (run B-314; Tables 2 and 3), we observed that with the use of a bulk composition slightly higher in CO_2 (DN-1; Table 1), than for example CMAS-CO_2-1 (run B-450; Tables 1 and 2), whole scale melting occurs, and a large amount of silicate glass is produced that coexists with forsterite; this just means that melting phase relations are starting-composition dependent. On the basis of these runs, we infer that the transition from carbonatitic to silicate melt at 2.8 GPa occurs around 1550 °C, and a similar melt transition is thought to be operational at 3 GPa in the temperature range of 1525–1575 °C.

Between 2 and 2.6 GPa and at temperatures higher than prevailing at the solidus ledge (Figure 9), carbonatite is no longer the only melt in the experiments. Forsterite, cpx, opx (although, see later), and spinel/garnet are found in equilibrium with two melts, which are silicate and carbonatitic in composition. Unlike the carbonatitic melt, the silicate melt shows some variation in composition as a function of temperature

(Table 3). Carbonatitic and silicate liquid as pairs disappear as the dry peridotite solidus in the system CMAS is approached. For instance, at temperatures above 1445 °C and 1475 °C at 2 and 2.2 GPa, and above 1500 °C at 2.4 and 2.6 GPa, (Figure 9), respectively, only silicate melt with approximately 10 wt % dissolved CO_2 (Table 3) is found in equilibrium with forsterite ± cpx ± opx ± vapor. On this basis, we suggest that the transition from two melts to a single silicate melt occurs over a narrow temperature range (Figure 9).

Additionally, save two experimental charges, B-455 and B-452, at 2.2 GPa/1460 °C and 2.4 GPa/1475 °C, respectively, (Table 2) so long as two melts are present, opx does not seem to be a stable crystalline phase in the experimental charges. Quite a few attempts, to saturate experimental charges containing two melts with opx, even employing several different starting compositions, did not succeed. For instance, starting compositions DN-1, DN-2, DN-8, DN-9, DN-10, and CMAS-CO_2-20 did not produce opx in the 2–2.6 GPa pressure range; yet two runs B-455 and B-452 (Table 2) are isobarically invariant and consist of the assemblage forsterite + opx + cpx + spinel + carbonatitic liquid + silicate liquid. In addition, *Keshav and Gudfinnsson* [2013] locate a P-T invariant point at 2 GPa and 1420 °C, which has two melts (carbonatitic and silicate in composition) plus forsterite, opx, cpx, spinel, and vapor. Hence, if the two experiments from the present study (B-455 and B-452) are evaluated together with the 2 GPa P-T invariance in *Keshav and Gudfinnsson* [2013], then most likely the melting phase relations involving forsterite + opx + cpx + spinel + carbonatitic liquid + silicate liquid would be P-T univariant from 2 to 2.6 GPa, and this univariant line would have to be on the P-T divariant surface between the solidus ledge (present study) and the solidus of dry, model peridotite in CMAS (Figure 9). On this basis, there are the following observations: (a) this P-T univariant line that contains two melts plus forsterite, opx, cpx, and spinel/garnet is the vapor-absent (Vap) reaction whose existence was speculated upon in the companion study [*Keshav and Gudfinnsson*, 2013]. In the companion study, the (Vap) reaction was written as opx + cpx + spinel + carbonatitic liquid = forsterite + silicate liquid and (b) the (Vap) reaction would have to commence from the 2 GPa P-T invariance [*Keshav and Gudfinnsson*, 2013]; this (Vap) reaction would also have to terminate somewhere between 2.6 and 2.8 GPa, for, in the present study there is only one liquid which is carbonatitic in composition over a fairly large temperature range at 2.8 GPa (Table 3 and Figure 9). The melting reaction calculated using the phase compositions from the runs B-455 and B-452 (Table 3) in the present study is 0.29 opx + 0.96 cpx + 0.11 spinel + 0.13 carbonatitic liquid = 0.50 forsterite + 1 silicate liquid. This reaction corresponds to the (Vap) reaction estimated in the study of *Keshav and Gudfinnsson* [2013].

We interpret the presence of two melts, on the P-T divariant surface bound between the ledge and the solidus of dry peridotite in CMAS (Figure 9), as due to liquid immiscibility. Thus far, immiscibility between carbonatites and silicate melts has been experimentally observed only in the presence of alkalies [*Brooker and Kjarsgaard*, 2011, and references therein; *Martin et al*., 2013, and references therein]. Over 2–2.6 GPa (Figure 9), the experimentally produced liquids show the following evolution: single carbonatite (along the ledge) − carbonatite + silicate melt − single silicate melt. We propose that carbonatite-silicate liquid immiscibility in the absence of alkalies, from direct melting of carbonated peridotite, is possible in the Earth's mantle. Indeed, it has been suggested that natural carbonatites containing relatively high concentrations of alkalies might not represent primary or near-primary carbonatitic magmas from the Earth's mantle [*Bailey*, 1989; *Bailey et al*., 2005, 2006]. These studies have questioned the validity of experiments wherein highly alkalic, dolomitic carbonatites have been claimed to be representative of primary carbonatitic magmas [*Wallace and Green*, 1988]. The immiscibility observed here in the system CMAS-CO_2 was not seen before, because this composition space was not previously explored (though see *Keshav and Gudfinnsson* [2013]).

8. Possible Implications of the Present Study

Carbonatites in natural settings are more calcic in composition [*Woolley and Kempe*, 1989] than seen in the experiments here, and the silicates associated with such natural calciocarbonatites range approximately from being melilititic to nephelinitic in composition [*Bailey et al*., 2005, 2006, and references therein]. The present experimental study did not contain alkalies, iron oxide, or water, components that might have an influence on the fusion relations. On this basis, a direct comparison of our data to the natural occurrences is not realistic. Yet *Bailey* [1989] described carbonatitic pyroclastic deposits from the Rufunsa valley in Zambia that contain iron-free melt droplets which are dolomite (molar Ca# = 50–52) in composition, which are similar to the carbonatitic liquid seen in the experiments here. Unlike in Spain [*Bailey et al*., 2005] or in France [*Bailey et al*., 2006], associated

silicate magmas at Rufunsa are absent [*Bailey*, 1989]. In Spain and in France, dolomite-calcite globules are associated with nephelinitic and melilititic lava fragments. On a model basis (that is, in CMAS-CO_2), the silicate liquids in the present set of experiments do correspond to them being somewhat melilititic and nephelinitic in composition; hence, dolomitic and silicate liquids in at least some natural settings might have formed through melt unmixing over the pressure range of 2 to 2.6 GPa. In this manner, two such compositionally different liquids might not be restricted only to near-solidus conditions, for experiments in this work demonstrate that two conjugate melts are present over a fair temperature range, and the temperature range over which two melts are present increases as a function of increasing pressure. Hence, the prevailing view from experimental petrology that immiscibility was unlikely at mantle pressures is unsupported from the present study. The possibility that conjugate melts might form at the very initiation of fusion of a carbonated mantle has been discussed in *Bailey et al*. [2006] and is based on the observation that quite large variations occur in the proportions of immiscible melts in different lava fragments; such variation in the proportions of immiscible melts might suggest two melts at the onset of fusion of carbonated peridotite, with eruption conditions being such that the two immiscible mantle melts avoided homogenization. The present experimental study provides support for this line of thought. In *Bailey et al*. [2006], melt unmixing can also happen when a single liquid depressurizes upon ascent, and this single liquid is a "highly carbonated silicate melt" (quotes, ours). Yet as documented here, whenever there is a single liquid (away from the solidus ledge), it is either a carbonatite or a silicate glass that is not "highly carbonated" (it is not clear from reading of *Bailey et al*. [2006] as to what might constitute a "highly carbonated silicate glass"). Instead, the single liquid (for instance, at 2.8 GPa) that could turn into two liquids with decreasing pressure (for instance, at 2.6 GPa) is a carbonatite. Therefore, on the basis of the present study it is highly likely that both the processes, a single liquid dissociating into two with depressurization, or two melts being present at the onset of fusion of carbonated mantle peridotite, might be operational in nature; the present experiments do not allow to distinguish one process from the other.

9. Conclusions

Melting phase relations of carbonated peridotite in the system CMAS-CO_2 from 2 to 3 GPa reveal that carbonatites, along the pressure-temperature univariant carbonated peridotite solidus ledge, are stable liquids to pressure as low as 2 GPa. There is a pressure-temperature divariant region over which carbonatite coexists with silicate liquid and peridotite crystalline phase assemblage and/or vapor from 2 to 2.6 GPa. The occurrence of these two compositionally distinct liquids is interpreted to be due to liquid immiscibility. On this basis we suggest that a similar unmixing of melts, in the absence of alkalies, might be operational at depths of about 60–80 km in the Earth.

Acknowledgments

The authors thank Hans Keppler for discussions related to the work presented here. The second author thanks Yaoling Niu, Edward Stolper, Hans Keppler, and Marjorie Wilson for their kind invitation to participate in Peter Wyllie-fest at the Goldschmidt Conference in Davos (2009), where initial part of this study was presented. Shaunak Ghosh acknowledges Bayerisches Geoinstitut, Germany, for a generous award of a graduate intern fellowship during the summer of 2008. A referee who wished to remain anonymous, Tahar Hammouda, and Journal Editor Michael Walter officially reviewed this manuscript and are thanked for their comments. Tahar Hammouda and Michael Walter did a lot of work to turn this manuscript into its present form, and the authors thank them for their efforts. Bayerisches Geoinstitut, Germany, and partial funding from the 7th framework CIG Marie-Curie grant (303301) from the EU to the second author supported the present study.

References

Bailey, K. (1989), Carbonate melt from the mantle in the volcanoes of south-east Zambia, *Nature*, *338*, 415–418.

Bailey, K., M. Garson, S. Kearns, and A. P. Velasco (2005), Carbonate volcanism in Calatrava, central Spain: A report on the initial findings, *Min. Mag.*, *69*, 901–915.

Bailey, K., S. Kearns, J. Mergoil, J. Daniel Mergoil, and B. Paterson (2006), Extensive dolomitic volcanism through the Limagne Basin, central France: A new form of carbonatite activity, *Min. Mag.*, *70*, 231–236.

Brenan, J., and E. B. Watson (1988), Fluids in the lithosphere, 2. Experimental constraints on CO_2 transport in dunite and quartzite at elevated P-T conditions with implications for mantle and crustal carbonation processes, *Earth Planet. Sci. Lett.*, *91*, 141–158.

Brooker, R. A., and B. Kjarsgaard (2011), Silicate-carbonate liquid immiscibility and phase relations in the system SiO_2-Na_2O-Al_2O_3-CaO-CO_2 at 0.1-2.5 GPa with application to carbonatite genesis, *J. Petrol.*, *52*, 1281–1305.

Buob, A., R. W. Luth, M. W. Schmidt, and P. Ulmer (2006), Experiments on $CaCO_3$-$MgCO_3$ solid solutions at high pressure and temperature, *Am. Mineral.*, *91*, 435–440.

Byrnes, A. P., and P. J. Wyllie (1981), Subsolidus and melting relations for the join $CaCO_3$-$MgCO_3$ at 10 kbar, *Geochim. Cosmochim. Acta*, *45*, 321–328.

Dalton, J. A., and D. C. Presnall (1998), Carbonatitic melts along the solidus of model lherzolite in the system CaO-MgO-Al_2O_3-SiO_2-CO_2, *Contrib. Mineral. Petrol.*, *131*, 123–135.

Eggler, D. H. (1974), Peridotite-carbonate relations in the system CaO-MgO-SiO_2-CO_2, in *Carnegie Inst. Washington Yearb*, vol. 74, pp. 468–474, Carnegie Institution of Washington, Washington, D. C.

Eggler, D. H. (1975), Composition of the partial melt of carbonated peridotite in the system CaO-MgO-SiO_2-CO_2, in *Carnegie Inst. Washington Yearb*, vol. 75, pp. 623–626, Carnegie Institution of Washington, Washington, D. C.

Eggler, D. H. (1976), Does CO_2 cause partial melting in the low-velocity layer of the mantle?, *Geology*, *4*, 69–72.

Eggler, D. H. (1978), The effect of CO_2 upon partial melting of peridotite in the system Na_2O-CaO-Al_2O_3-MgO-SiO_2-CO_2, *Am. J. Sci.*, *278*, 305–343.

Eggler, D. H. (1987a), Discussion of recent papers on carbonated peridotite, bearing on metasomatism and magmatism: An alternative, *Earth Planet. Sci. Lett.*, *82*, 398–400.

Eggler, D. H. (1987b), Discussion of recent papers on carbonated peridotite, bearing on metasomatism and magmatism: Final comment, *Earth Planet. Sci. Lett.*, *82*, 403.
Eggler, D. H., J. R. Holloway, and B. O. Mysen (1976), High CO_2 solubilities in mantle magmas: Comment, *Geology*, *4*, 198–199.
Gudfinnsson, G. H., and D. C. Presnall (1996), Melting relations of model lherzolite in the system CaO-MgO-Al_2O_3-SiO_2 at 2.4-3.4 GPa and the generation of komatiites, *J. Geophys. Res.*, *101*, 27,701–27,709.
Gudfinnsson, G. H., and D. C. Presnall (2005), Continuous gradations among primary carbonatitic, kimberlitic, melilitic, basaltic, picritic, and komatiitic melts in equilibrium with garnet lherzolite at 3–8 GPa, *J. Petrol.*, *46*, 1645–1659.
Hammouda, T. (2003), High-pressure melting of carbonated eclogite and experimental constraints on carbon cycling and storage in the mantle, *Earth Planet. Sci. Lett.*, *214*, 357–368.
Irving, A. J., and P. J. Wyllie (1975), Subsolidus and melting relationships for calcite, magnesite, and the join $CaCO_3$-$MgCO_3$ to 36 kb, *Geochim. Cosmochim. Acta*, *39*, 35–53.
Keppler, H., and D. J. Frost (2005), Introduction to minerals under extreme conditions, in *EMU Notes in Mineralogy, 7*, edited by R. Miletich, pp. 1–30 , Eötvös Univ. Press, Budapest, Hungary.
Keshav, S., and G. H. Gudfinnsson (2013), Silicate liquid-carbonatitic liquid transition along the melting curve of model, vapor-saturated peridotite in the system CaO-MgO-Al_2O_3-SiO_2-CO_2 from 1.1 to 2 GPa, *J. Geophys. Res. Solid Earth*, *118*, 3341–3353, doi:10.1002/jgrb.50249.
Klemme, S., and H. S. O'Neill (2000), The near-solidus transition from garnet lherzolite to spinel lherzolite, *Contrib. Mineral. Petrol.*, *138*, 237–248.
Liu, T.-C., and D. C. Presnall (2000), Liquidus phase relations in the system CaO-MgO-Al_2O_3-SiO_2 at 2.0 GPa: Applications to basalt fractionation, eclogites, and igneous sapphirine, *J. Petrol.*, *41*, 3–20.
Longhi, J. (2005), Temporal stability and pressure calibration of barium carbonate and talc/pyrex pressure media in a piston-cylinder apparatus, *Am. Mineral.*, *90*, 206–218.
Luth, R. W. (1999), Carbon and carbonates in the mantle, in Mantle Petrology: Field observations and high pressure experimentation, A tribute to F.R. (Joe) Boyd, *Geochem. Soc. Spec. Publ.*, *6*, 297–316.
Luth, R. W. (2006), Experimental study of the $CaMgSi_2O_6$-CO_2 system at 3–8 GPa, *Contrib. Mineral. Petrol.*, *151*, 141–157.
Martin, L., M. W. Schmidt, H. B. Mattsson, and D. Guenther (2013), Element partitioning between immiscible carbonatite and silicate melts for dry and H_2O-bearing systems at 1–3 GPa, *J. Petrol.*, *54*, 2301–2338.
Milholland, C. S., and D. C. Presnall (1998), Liquidus phase relations in the system CaO-MgO-Al_2O_3-SiO_2 at 3.0 GPa: The aluminous pyroxene thermal divide and high-pressure fractionation of picritic and komatiitic magmas, *J. Petrol.*, *39*, 3–27.
Presnall, D. C. (1986), An algebraic method for determining equilibrium crystallization and fusion paths in multicomponent systems, *Am. Mineral.*, *71*, 1061–1070.
Presnall, D. C., J. R. Dixon, T. H. O'Donnell, and S. A. Dixon (1979), Generation of mid-ocean ridge tholeiites, *J. Petrol.*, *20*, 3–35.
Wallace, M. E., and D. H. Green (1988), An experimental determination of primary carbonatite magma composition, *Nature*, *335*, 343–346.
Walter, M., et al. (2002), Spinel-garnet lherzolite transition on the system CaO-MgO-Al_2O_3-SiO2 revisited: An in situ X-ray study, *Geochim. Cosmochim. Acta*, *66*, 2109–2121.
Watson, E. B., and J. Brenan (1987), Fluids in the lithosphere, 1. Experimentally-determined wetting characteristics of CO_2-H_2O fluids and their implications for fluid transport, host-rock physical properties, and fluid inclusion formation, *Earth Planet. Sci. Lett.*, *85*, 497–515.
White, B. S., and P. J. Wyllie (1992), Solidus reactions in synthetic lherzolite-H_2O-CO_2 from 20–30 kbar, with applications to melting and metasomatism, *J. Volcanol. Geotherm. Res.*, *50*, 117–130.
Woermann, E., and M. Rosenhauer (1985), Fluid phases and the redox state of the Earth's mantle: Extrapolations based on experimental, phase-theoretical, and petrological data, *Fortsch. der Mineral.*, *63*, 263–349.
Woolley, A. R., and D. R. C. Kempe (1989), Carbonatites: Nomenclature, average chemical compositions, and element distribution, in *Carbonatites: Genesis and Evolution*, edited by K. Bell, pp. 1–14 , Unwin, London, U. K.
Wyllie, P. J. (1987a), Discussion of recent papers on carbonated peridotite, bearing on mantle metasomatism and magmatism, *Earth Planet. Sci. Lett.*, *82*, 391–397.
Wyllie, P. J. (1987b), Discussion of recent papers on carbonated peridotite, bearing on mantle metasomatism and magmatism: Response, *Earth Planet. Sci. Lett.*, *82*, 401–402.
Wyllie, P. J., and W. L. Huang (1975), Influence of mantle CO_2 in the generation of carbonatites and kimberlites, *Nature*, *257*, 297–299.
Wyllie, P. J., and W. L. Huang (1976a), Carbonation and melting reactions in the system CaO-MgO-SiO_2-CO_2 at mantle pressures with geophysical and petrological applications, *Contrib. Mineral. Petrol.*, *54*, 79–107.
Wyllie, P. J., and W. L. Huang (1976b), High CO_2 solubilities in mantle magmas, *Geology*, *4*, 21–24.

Erratum

In the originally published version of this article, the information in the columns of table 4 were printed incorrectly. Table 4 has since been corrected and this version may be considered the authoritative version of record.